Journal of Stored Products Research 116 (2026) 102958

Contents lists available at ScienceDirect

Journal of Stored Products Research

journal homepage: www.elsevier.com/locate/jspr

An efficient chitinase from *Bacillus amyloliquefaciens* M6: Immobilization to ZnO/RGO nanocomposite and its application in biocontrol

Sevda Uçar [a], Neslihan Dikbaş [b,*], Şeyma Alım [b], Emir Çepni [c], Göksel Tozlu [d], Merve Şenol Kotan [b], Tuba Öznülüer Özer [e], Muhammed Tatar [a], Kağan Kökten [a], Tolga Karaköy [f], Barış Binay [g]

[a] *Sivas Science and Technology University, Faculty of Agricultural Sciences and Technology, Department of Field Crops, Sivas, Turkey*
[b] *Ataturk University, Faculty of Agricultural, Department of Agricultural Biotechnology, Erzurum, Turkey*
[c] *Ataturk University, Faculty of Engineering, Department of Electrical and Electronics Engineering, Erzurum, Turkey*
[d] *Ataturk University, Faculty of Agricultural, Department of Plant Protection, Erzurum, Turkey*
[e] *Ataturk University, Faculty of Science, Department of Analytical Chemistry, Erzurum, Turkey*
[f] *Sivas Science and Technology University, Faculty of Agricultural Sciences and Technology, Department of Plant Protection, Sivas, Turkey*
[g] *Gebze Technical University, Department of Bioengineering, Gebze, Kocaeli, Turkey*

ARTICLE INFO

Keywords:
Bacillus
chitinase
ZnO/RGO nanocomposite
Rhyzopertha dominica
Oryzaephilus surinamensis
Biocontrol agent

ABSTRACT

In this study, the chitinase enzyme purified from *Bacillus amyloliquefaciens* M6 was immobilized on Zinc oxide/reduced graphene oxide nanocomposites (ZnO/RGO NCs), and its activity on *Rhyzopertha dominica* and *Oryzaephilus surinamensis* was tested. To optimize the culture medium, the M6 strain was developed under varying conditions, and the optimum substrate concentration, temperature, pH, and incubation time for chitinase production were determined as 5 g/L chitin, 35 °C, 6.0 pH, and 24 h. Compared to its activity prior to optimization (10.42 U/mL), the chitinase activity of the strain was observed to increase by 2.2 times. Under these conditions, chitinase was purified 6.75-fold from strain M6 with a specific activity of 228.90 U/mg (activity: 11,48 U/mL) and a yield of 1.84 %, and its molecular weight was determined to be ~50 kDa. Chitinase was immobilized on ZnO/RGO NCs with 99.68 % immobilization efficiency and 94.30 % recovered activity. The optimum pH and temperature values of free and immobilized chitinase were determined as 6.0 and 45 °C. The activity of immobilized chitinase against *R. dominica* and *O. surinamensis* was tested and the LC_{50} and LC_{90} values for *R. dominica* were calculated as 1.8 mg/mL (32.8 U/mL) and 3.8 mg/mL (69.2 U/mL) and 4.8 mg/mL (87.4 U/mL) and 10.0 mg/mL (182.0 U/mL) for *O. surinamensis*. Thus, the obtained results concluded that the immobilized chitinase proved an alternative biocontrol agent to hazardous synthetic pesticides, the application of this biocontrol agent to make biopesticides will prove more reliable for sustaining the crop productivity and in crop protection.

1. Introduction

Cereals are one of the most important agricultural products that constitute the main component of human food and animal feed due to the presence of valuveable nutrients such as lipids, carbohydrates, proteins, minerals and vitamins (Los et al., 2020). The worldwide importance and widespread use of cereal grains and products need the quick action in preservation and decontamination of cereals (Mir et al., 2021). Although, several factors affecting the quality of cereals during storage conditions, and the pathogens and storage pests are the main ones (Sirohi et al., 2021). *R. dominica*, a cosmopolitan primary pest, causes significant economic losses in cereals globally, especially in wheat, barley and rice crops (Hassan et al., 2021). *R. dominica* attacks the internal part of the grains and converts the grains into flour (Sabbour, 2020). Afterthat, the *O. surinamensis* is an important secondary stored grain pest, that feeding on cereal grains cause the damage and contamination in stored rice, flour, dried fruit, tobacco and vegetables (Hashem et al., 2021; del Arco et al., 2024). Losses caused by cereal pests during storage are estimated to be 5 %–10 % worldwide and up to 40 % has been reported in just developing countries (Huang et al., 2022).

* Corresponding author.
E-mail address: neslidikbas@atauni.edu.tr (N. Dikbaş).

https://doi.org/10.1016/j.jspr.2026.102958
Received 8 September 2025; Received in revised form 19 January 2026; Accepted 19 January 2026
Available online 22 January 2026
0022-474X/© 2026 Elsevier Ltd. All rights are reserved, including those for text and data mining, AI training, and similar technologies.

Although various control methods such as synthetic pesticides, solarization, fumication with plant parts have been developed and applied previously to prevent from the diseases and pests (Tudi et al., 2021). However, excessive or unnecessary use of pecticides at inappropriate times leads to the accumulation of pesticide residues in processed cereals, cause direct or indirect effects on the environment and human health, biodiversity loss, contaminate the fresh air and water (Ngegba et al., 2022; de Sousa et al., 2023; Kaur et al., 2024). There is a dire need to develop an alternate to the reported methods (Swathy et al., 2024; El Aalaoui et al., 2025). Therefore, the application of the microbial enzyme as biocontrol agents prove most effective to control these destructive pests (Dikbaş et al., 2021; Berini et al., 2024). The most striking enzyme family among these is chitinases. Chitinases are enzymes belonging to the hydrolases group, obtained from many prokaryotic and eukaryotic organisms, that have the potential to break down chitin, the main component of insect exoskeletons and fungal cell walls (Ezzine et al., 2024). Moreover, chitinase-based enzymatic method is likely to be a more efficient and sustainable method for controlling the insect pest, due to there friendly compatiblity with environment, and human health. However, the stability of these enzyme is the main hinder in its broader application. Immobilized enzymes have a higher resistance to environmental changes and can easily recycled (Tülek, 2025).

The large surface area-to-volume ratios, high biocompatibility, and physicochemical properties of nanomaterials make them a preferred option for enzyme immobilization. Various nanomaterials, including metal and metal oxide (MO) nanoparticles, carbon-based materials, and polymeric nanoparticles, have been widely investigated for enzyme immobilization (Singh et al., 2025; Tülek et al., 2025). Among MO nanoparticles, zinc oxide nanoparticles (ZnO NPs) are more attractive support matrices that allow for easy immobilization of enzymes without significantly altering their structure or activity, due to their non-toxicity, low cost, high isoelectric point, high surface area, chemical and thermal resistance, and biocompatibility (Hassanisaadi et al., 2022; Ahmed et al., 2023; Khalid et al., 2023). Previous studies have shown that ZnO NPs can be successfully used in the immobilization of various enzymes (Pekdemir et al., 2024; Sadi et al., 2025). In addition to ZnO NPs, graphene-based materials such as graphene oxide (GO) and reduced graphene oxide (RGO) exhibit versatility in enzyme immobilization due to their high surface area, pore volume size, good adsorption ability, electrical conductivity, flexibility, chemical and thermal stability, eco-friendliness, and exceptional mechanical strength, and provide enhanced catalytic performance, stability, and reusability compared to previous materials (Priyadarshi and Singhal, 2025; Singh et al., 2025). The combined use of MO/RGO nanocomposites exhibits better material properties compared to single MO or single RGO components due to the combined effect of both (Aparna and Rakhi, 2025). Therefore, ZnO/RGO nanocomposites formed by combining ZnO with RGO form hybrid systems that are highly suitable for enzyme immobilization in terms of both structural and surface properties.

There are different physical, chemical and biological methods in the literature for the synthesis of nanoparticles (Altammar, 2023; Jamil et al., 2025). Physical methods are often expensive and energy-consuming procedures, while chemical methods use chemicals that are harmful to the environment. In recent years, green synthesis approaches that minimize environmental impacts, reduce the use of toxic chemicals and prioritize energy efficiency have emerged as a strong alternative to conventional methods in nanomaterial production (Aasim et al., 2025; Alsafran et al., 2025).

In the present study, chitinase enzyme was purified from *Bacillus amyloliquefaciens*, immobilized into ZnO/RGO NCs synthesized from garlic (*Allium sativum*) extract by green synthesis method, and nanobioformulation was formed. Then, the efficacy of the formulation against two storage pests (*R. dominica* and *O. surinamensis*) that cause significant yield losses in agricultural production was revealed.

2. Materials and methods

2.1. B. amyloliquefaciens

B. amyloliquefaciens M6 (Former culture code: M6, Accession number: KX249603) used in the study is kept at −80 °C in the culture collection of Prof. Dr. Neslihan Dikbaş at Atatürk University, Faculty of Agriculture, Department of Agricultural Biotechnology.

2.2. Preparation of colloidal chitin

Firstly, 5 g of chitin was treated with 75 mL of concentrated HCl and stirred overnight at 4 °C on a magnetic stirrer. Afterthat, the cold ethanol (50 %) was added to the suspension and kept at room temperature while stirring overnight. The suspension was washed with cold distilled water (−4 °C) adjusted to pH 7.0 and centrifuged at 12,000 rpm for 25 min after each wash. Colloidal chitin was taken on filter paper and allowed to dry (Ong et al., 2017).

2.3. Optimization of chitinase production

Optimization of chitinase production was performed according to Ong et al. (2017) and Das et al. (2012) with some minor modifications. Optimization was performed based on substrate concentration, culture time, temperature, and pH. Strain M6 was inoculated into Nutrient broth (NB) containing different concentrations of colloidal chitin (0, 5, 10, 15, and 20 g/L) and incubated at 30 °C, 150 rpm for 7 days. Chitinase activity was analyzed from samples taken every 24 h and the culture time and substrate concentration at which enzyme production peaked were determined. In order to determine the pH and incubation temperature at which M6 exhibits optimum chitinase activity, the strain was cultured at different pH values (5, 6, 7, 8, 9 and 10) and temperatures (20, 25, 30, 35 and 40 °C) and chitinase activity was measured. The cultures were centrifuged at 10,000 rpm for 14 min and the supernatant was used for chitinase assay. At each pH and temperature range, viable bacteria were counted and the pH and temperature value at which the M6 strain showed optimum growth was determined.

2.4. Determination of chitinase activity

Chitinase activity was determined by analyzing the amount of N-Acetylglucosamine (GlcNAc) released from colloidal chitin. 0.5 mL of the enzymatic solution was mixed with 0.5 mL of citrate buffer (20 mM, pH: 6.0) containing 0.2 % chitin and incubated at 30 °C for 30 min. The amount of reducing sugar was determined by the DNS method (Miller, 1959) and one unit of chitinase activity was defined as the amount of enzyme producing 1 mol of reducing sugar in the form of GlcNAc per minute under the above conditions (Laribi-Habchi et al., 2020).

2.5. Purification of chitinase

Strain M6 was incubated in NB containing 5 % colloidal chitin for 24 h at 35 °C and then centrifuged at 10,000 rpm for 30 min at 4 °C. The supernatant was fractionally precipitated with ammonium sulfate at 0–80 %. The enzyme solution was transferred to a dialysis bag and dialyzed against 10 mM sodium citrate buffer (pH 6.0). The dialysed suspension was loaded onto a DEAE-Sephadex ion exchange column (2.5 × 30 cm) pre-equilibrated with 20 mM sodium citrate (pH 6.0). The column was washed with the same buffer and then bound proteins were separated by applying a gradient between 0 and 1 M NaCl to the column (Senol et al., 2014). The amount of protein in the purified enzyme solution was determined by the Bradford (1976) method and the molecular weight of the enzyme was determined by Matrix-assisted laser desorption ionization-time-of-flight-mass spectrometry (MALDI--TOF-MS) and SDS PAGE analysis (Krolicka et al., 2018).

2.6. Synthesis of ZnO/RGO NCs

The synthesis of ZnO/RGO NC was carried out by a green method using $Zn(NO_3)_2$ and GO as Zn and RGO precursors, respectively, and garlic extract as a reductant and stabilizer. For this purpose, garlic extract was obtained from commercially available garlic by maceration process (Ahamed et al., 2022). 25 g of $Zn(NO3)_2{\cdot}6H_2O$ and 0.5 g of GO were added to 500 mL of garlic extract and the mixture was stirred using a magnetic stirrer for 1 h. Next, the mixture was kept in a water bath at 60 °C for 1 h to ensure particle growth and then dried in an oven at 150 °C for 1 h. The resulting precipitate was washed several times with deionized water and annealed at 400 °C for 1 h. After the annealing process, the green synthesis of ZnO/RGO NC was completed (Fig. 1).

2.7. Structural and morphological characterization of ZnO/RGO NCs

For the structural characterization of green synthesized ZnO/RGO NCs, X-ray photoelectron spectroscopy (XPS, Specs-Flex, Al anode), energy dispersive X-ray spectroscopy (EDS), X-ray diffraction spectroscopy (XRD), fourier transform infrared spectroscopy (FT-IR), Raman spectroscopy and ultraviolet–visible spectroscopy (UV–VIS) techniques were used. Shape and size determinations were analyzed by scanning electron microscopy (SEM) and transmission electron microscopy (TEM) for the morphological characterization of nanocomposite.

2.8. Immobilization of chitinase by ZnO/RGO NCs

Chitinase was immobilized on ZnO/RGO NC by adsorption followed by crosslinking. To 1 mL of chitinase solution containing 0.5 mg protein, 1 mL ZnO/RGO NC (5 mg/mL) was added and adsorption was carried out by shaking slowly at 100 rpm for 20 min at room temperature. Then 2 % glutaraldehyde (v/v) was added to the solution for crosslinking and shaken at 100 rpm for 15 min. At the end of the time, the solution was collected by centrifugation at 5000×*g* for 10 min and the filtrate was used for protein assay. Immobilized chitinase was stored at 4 °C until use. Immobilization efficiency and recovered activity were determined using the following formulas (Tülek et al., 2021).

$$\text{Immobilization Yield } (\%) = \frac{(PT - PF)}{PT} x100$$

Where; P_T is the amount of protein initially added (mg), P_F is the amount of protein in the collected filtrates (mg).

The recovered activity was calculated using the following formula:

$$\text{Recovered Activity } (\%) = \frac{Ui}{Ut} x100$$

Where U_i and U_t are the activity of immobilized chitinase and the total activity of the loaded chitinase, respectively.

2.9. Lyophilization

Lyophilization was carried out through sequential steps consisting of freezing at −30 °C for 15 min, VP heating at −45 °C for 15 min, followed by primary drying at −85 °C for 20 h under vacuum conditions (vacuum pressure: 0.630 mbar; safety pressure: 1.30 mbar), and secondary drying at −75 °C for 4 h (vacuum pressure: 0.500 mbar; safety pressure: 1.30 mbar) (Ó'Fágáin, 2004).

2.10. Effect of temperature and pH on the activity of free and immobilized chitinase

In order to determine the temperature at which free and immobilized chitinase exhibited optimum activity, activity was measured in the range of 15–85 °C in 5 °C increments. Reaction temperatures were adjusted using a water bath and chitinase activity was determined by absorbance measurement at 540 nm wavelength (Dikbaş et al., 2021). The effect of pH on activity was determined by measuring activity at different pH ranging from 2.0 to 11.0. Sodium acetate (pH 2.0–3.0), sodium citrate (pH 4.0–6.0), Tris (pH 7.0–9.0), and sodium carbonate (pH 10.0–11.0) buffers were used to determine the optimum pH.

2.11. Insecticidal activity of immobilized chitinase

The efficacy of the nanobioformulation (immobilized chitinase) against *R. dominica* and *O. surinamensis* adults was determined in the laboratory. The experiment was carried out in a random plots experimental design according to the Ministry of Food, Agriculture and Livestock's Standard Pesticide Trial Method for Pests in Warehouses (GDARP, 2024). Different nanobioformulation doses (*R. dominica* (0.5 mg/mL (9.1 U/mL), 1 mg/mL (18.2 U/mL), 1.5 mg/mL (27.3 U/mL), 2 mg/mL (36.4 U/mL), 4 mg/mL (72.8 U/mL), and 6 mg/mL (109.2 U/mL)), *O. surinamensis* (2 mg/mL (36.4 U/mL), 4 mg/mL (72.8 U/mL), 6 mg/mL (109.2 U/mL), 8 mg/mL (145.6 U/mL), 10 mg/mL (182.0 U/mL), and 12 mg/mL (218.4 U/mL))) were sprayed into 250 cm^3 glass jars, each containing 50 g wheat grains. Treatment doses were determined based on preliminary trials. In addition, the chemical pesticide Deltamethrin 25 g/L + Piperonly Butoxide 250 g/L (EC (Emulsion concentrate)) used in the control of these pests and chitinase, ZnO NPs, RGO, ZnO/RGO NCs, and water were applied as controls to determine the effects of the substances used in immobilization. Twenty-five 1–7 day old test insects (including control treatments) were released into each jar 24 h after treatment of the immobilized enzyme to wheat grains. The jars were kept at 25 ± 1 °C and 60 % ± 5 % relative humidity. Samples were checked daily and dead and live insects were counted over time. The current treatments were performed separately for both insects and in three replicates. Corrected mortality rates were determined using the Abbott formula (Abbott, 1987).

2.11.1. Morphologic observations

The contact effect of the treatments on the insect (morphological changes) was determined by examining the insect cuticle and gut using SEM and stereo microscopy as described by Yu et al. (2015).

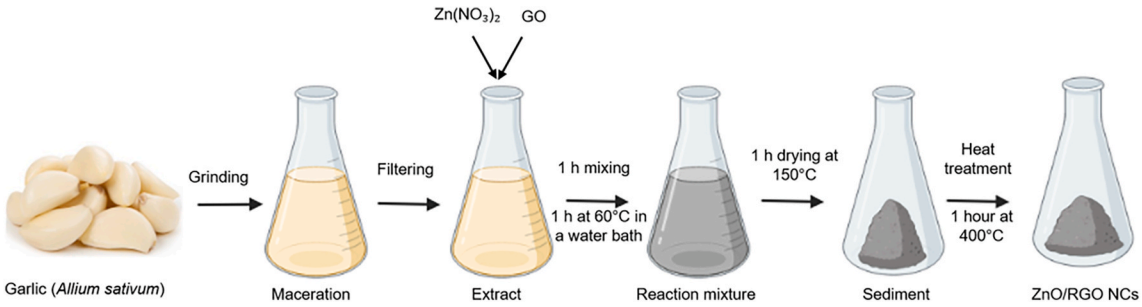


Fig. 1. Schematic of the green synthesis process of ZnO/RGO nanocomposite.

2.11.2. Intestinal enzyme profile

The digestive tract of treated dead insects was dissected with a fine-tipped needle under a microscope (Leica EZ4). Alkaline phosphatase (ALP), lactate dehydrogenase (LDH), and adenosine triphosphatase (ATPase) activities were determined using the methods described by Dikbaş et al. (2023).

2.12. Statistical analysis

Data were analyzed with IBM SPSS V23 and Minitab V14. Compliance with normal distribution was examined by Shapiro-Wilk test. Data were subjected to analysis of variance and multiple comparisons were determined by Tukey HSD test. Kruskal-Wallis test was used to compare mortality rates that were not normally distributed according to treatments and multiple comparisons were analyzed by Dunn's test. Probit regression analysis was used to determine the lethal dose and duration. Analysis results were presented as mean ± standard deviation and median (minimum - maximum) for quantitative data. Significance level was taken as $p < 0.050$. Independent sample *t*-test was used for the evaluation of intestinal enzyme activities.

3. Results and discussion

3.1. Optimization of chitinase production

Environmental factors such as nutrient sources and growing conditions play a vital role on microbial enzyme production activity (Philip et al., 2020). In the present study, different colloidal chitin concentrations (5, 10, 15, and 20 g/L) were investigated to ensure maximum chitinase production by *B. amyloliquefaciens* M6 and the highest enzyme activity was measured at 5 g/L colloidal chitin was added to the medium. The difference between this concentration and other concentrations was statistically significant ($p < 0.05$) (Table 1). It was observed that enzyme activity decreased at higher chitin concentrations (10, 15, and 20 g/L). This situation can be explained by substrate inhibition occurring at high colloidal chitin concentrations, as also noted in previous studies by Govindaraj et al. (2025). Similarly, it was reported that *B. pumilus* JUBCH08 showed maximum chitinase activity when the culture medium was supplemented with 0.5 % (w/v) colloidal chitin and chitinase activity decreased as the chitin concentration increased (Bhattacharya et al., 2016). Abirami et al. (2016) reported that colloidal chitin concentration in the range of 0.5–1 % significantly increased the chitinase production of *B. licheniformis* SSCL10. In addition, *B. licheniformis* strain B307 showed the highest chitinase activity in culture medium containing 0.5 % colloidal chitin (Akeed et al., 2020). *B. thuringiensis* LS1 (Sudha, 2020), *B. cereus* LS2 (Sudha, 2020), and *Bacillus cereus* GS02 (Dukariya & Kumar, 2020) strains exhibited optimum chitinase activity in a medium containing 1 % colloidal chitin. The findings and literature studies show that chitinase production is affected by the concentration of colloidal chitin in the medium.

The optimum fermentation time for chitinase production can vary depending on the organism, its growth type, the substrate, and other process parameters (Poria et al., 2021). To determine the incubation period associated with optimum chitinase acitivity, *B. amyloliquefaciens* was cultured in liquied medium for 7 days and enzyme activity was measured at 24 h intervals. The highest chitinase activity was observed after 24 h of incubation, revealed a statistically significant difference compared with activities recorded at later time points (48, 72, 96, 120, 144, and 168 h) ($p < 0.05$). Chitinase activity progressively decreased with increasing incubation duration as described in Table 1. In contrast to the results obtained, *B. cereus* GS02 showed maximum chitinase activity after 48 h, *B. amyloliquefaciens* SM3, and *B. thuringiensis* LS1 after 72 h of incubation (Kumar, 2012; Sudha, 2020; Dukariya & Kumar, 2020). In addition, *B. cereus* strain LS2 exhibited optimum chitinase activity at 96 h, *B. subtilis* strain SBMP4 at day 5, and *B. licheniformis* strain B307 at day 14 (Akeed et al., 2020; Sudha, 2020; Deeba et al., 2022). Thus, the comparison of the present study results with previous studies concluded that *B. amyloliquefaciens* M6 strain yielded optimum chitinase activity in a shorter incubation period. This could lead to more efficient use of resources and shorter fermentation times in industrial production, making *B. amyloliquefaciens* M6 a desirable target for bacterial chitinase production.

In order to determine the effect of incubation temperature on chitinase production, *B. amyloliquefaciens* M6 was grown at different temperatures in 5 intervals (20, 25, 30, 35, and 40 °C), and chitinase activity and viability were determined at each temperature. The optimum temperature 35 °C recorded best the fast strain growth and showed the highest chitinase activity (Fig. 2a and b). Viability and enzyme production gradually increased from 25 °C to 30 °C and from 30 °C to 35 °C, while they decreased significantly at 40 °C. In line with our results, *B. amyloliquefaciens* showed maximum chitinase activity at 35 °C in SM3 (Kumar, 2012). In addition, many researchers have reported that the optimum temperature for chitinase production by various *Bacillus* species is 30–37 °C (Bhattacharya et al., 2016; Gupta et al., 2017; Sudha, 2020).

In order to determine the pH at which *B. amyloliquefaciens* M6 showed maximum chitinase activity, the strain was grown in culture media adjusted to different pHs (4,5,6,7,8,9 and 10), and viability and activity were measured. M6 showed the highest viability and chitinase activity at pH 6 and activity and viability decreased significantly below/above this value (Fig. 2c and d). In parallel with the study, *B. subtilis* SBMP4, *B. licheniformis* B307, and *B. cereus* GS02 strains also showed optimum chitinase activity in an acidic medium (pH 5.5–6.5) (Akeed et al., 2020; Mohammed, 2020; Dukariya & Kumar, 2021). Bacteria showing optimum chitinase activity at neutral and alkaline pH have also been reported (Sudha, 2020; Cahyaningtyas et al., 2021; Harvinda et al., 2023).

The chitinase activity of the M6 strain, developed under optimal conditions determined after optimization of the culture medium, was measured as 22.38 U/mL. Compared to its activity prior to optimization (10.42 U/mL), the chitinase activity of the strain was observed to increase by 2.2 times. The increase in activity observed after optimization

Table 1
The amount of colloidal chitin and the incubation period at which *B. amyloliquefaciens* M6 exhibited optimum chitinase activity.

Collodial Chitin Amount (g/L)	h						
	24	48	72	96	120	144	168
	Activity (U/mL) ± SD	Activity (U/mL) ± SD	Activity (U/mL) ± SD	Activity (U/mL) ± SD	Activity (U/mL) ± SD	Activity (U/mL) ± SD	Activity (U/mL) ± SD
0 g/L	$12.7 \pm 0.1^{E,a}$	$12.4 \pm 0.0^{D,b}$	$12.4 \pm 0.1^{C,b}$	$10.8 \pm 0.1^{E,c}$	$9.9 \pm 0.1^{E,e}$	$10.3 \pm 0.1^{A,d}$	$9.3 \pm 0.1^{C,f}$
5 g/L	$24.7 \pm 0.1^{A,a}$	$14.6 \pm 0.1^{A,b}$	$13.3 \pm 0.1^{A,d}$	$14.1 \pm 0.0^{B,c}$	$10.5 \pm 0.1^{D,e}$	$10.2 \pm 0.1^{AB,f}$	$9.1 \pm 0.1^{D,g}$
10 g/L	$17.3 \pm 0.1^{C,a}$	$13.2 \pm 0.1^{C,b}$	$12.6 \pm 0.1^{B,c}$	$13.2 \pm 0.1^{C,b}$	$11.6 \pm 0.1^{A,d}$	$9.8 \pm 0.1^{C,e}$	$9.8 \pm 0.1^{B,e}$
15 g/L	$16.2 \pm 0.0^{D,a}$	$12.4 \pm 0.1^{D,c}$	$11.4 \pm 0.1^{E,d}$	$12.8 \pm 0.1^{D,b}$	$10.7 \pm 0.0^{C,e}$	$9.8 \pm 0.0^{C,g}$	$10.2 \pm 0.1^{A,f}$
20 g/L	$19.7 \pm 0.1^{B,a}$	$14.2 \pm 0.1^{B,c}$	$11.7 \pm 0.1^{D,d}$	$15.0 \pm 0.1^{A,b}$	$10.9 \pm 0.1^{B,e}$	$10.1 \pm 0.1^{B,f}$	$9.8 \pm 0.0^{B,g}$

According to the HSD Tukey multiple comparison test, capital letters in the table represent differences within each column, and lowercase letters represent differences within each row, **SD:** Standard deviation.

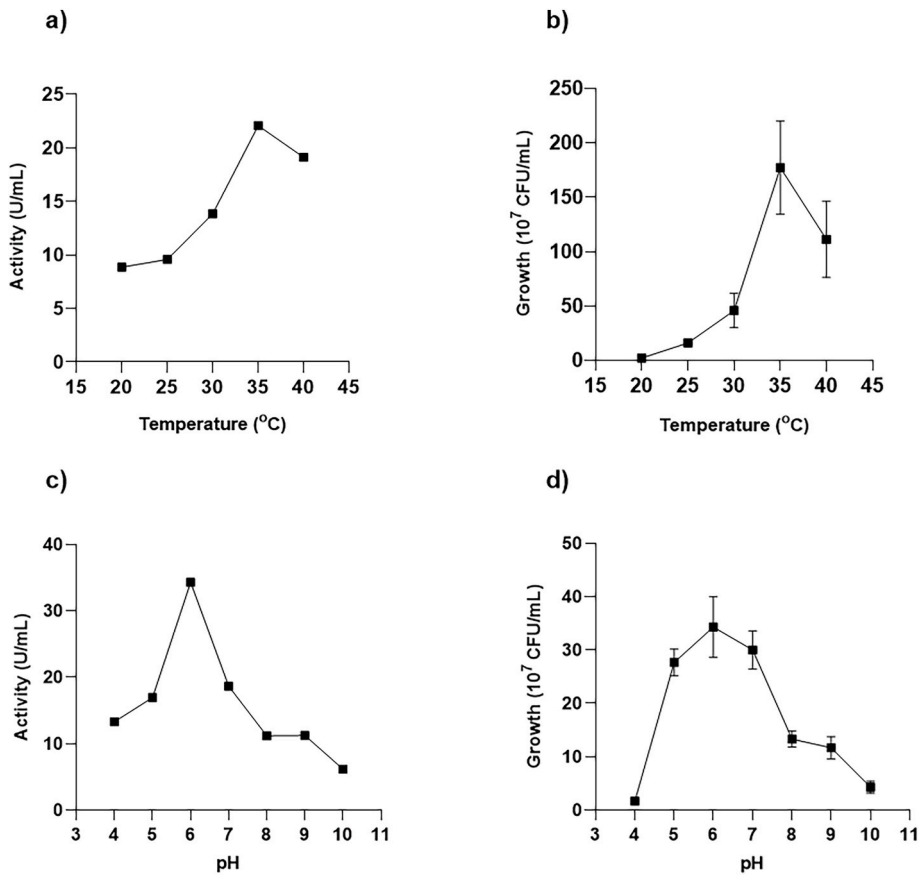


Fig. 2. Effect of temperature on chitinase production by *B. amyloliquefaciens* M6 (Error bars are not visible because the standard error values are too low) **(a)**; Effect of temperature on the growth of M6 **(b)**; Effect of pH on chitinase production by *B. amyloliquefaciens* M6 (Error bars are not visible because the standard error values are too low) **(c)**; Effect of pH on the growth of M6 **(d)**.

is consistent with studies in the literature showing that optimizing culture parameters can significantly increase activity (Adetiloye et al., 2025; Hazare et al., 2025).

3.2. Purification of chitinase

Chitinase enzyme from *B. amyloliquefaciens* was first purified 6.75-fold with a yield of 1.84 % using ammonium sulfate precipitation followed by DEAE-Sephadex ion exchange chromatography (Table 2). Although the yield decreased after purification, the purification process increased both the purity and specific activity of the enzyme. The specific activity of the purified chitinase was measured as 228.90 U/mg. Strain M6 showed higher specific activity than many chitinase-producing bacteria in the literature (*B. subtilis* B3, *B. cereus* NK91, *B. haynesii*, *B. licheniformis*) (Brzezinska et al., 2020; Essghaier et al., 2021; Thakur et al., 2022a; Govindaraj et al., 2024). The molecular weight of the purified chitinase was determined as ~50 kDa by SDS-PAGE and MALDI-TOF-MS (Fig. 3). The molecular weight of the enzyme is similar to chitinases purified from *B. thuringiensis* R 176 (47 kDa), *P. xylanexedens* Z2-4 (52.8 kDa) *B. subtilis* TD11 (55 kDa) (Chaiharn et al., 2019; Zhang et al., 2021; Malik et al., 2023). Chitinases with lower (*B. subtilis* B3 (37 kDa), *B. haynesii* (35 kDa), *B. thuringiensis* B-387 (40 kDa)) or higher (*B. cereus* BSH-4 (60 kDa), *B. licheniformis* SSCL-10 (66 kDa)) molecular weights have also been reported from different *Bacillus* species (Brzezinska et al., 2020; Sasi et al., 2020; Aktuganov et al., 2022; Hungund et al., 2022; Govindaraj et al., 2024). In addition, many researchers have reported that the molecular weight of chitinases obtained from bacterial sources varies between 30 and 80 kDa (Akeed et al., 2020; Thakur et al., 2022a). The results obtained showed that the chitinase purified from strain M6 is a monomeric enzyme like a number of chitinases available in the literatüre (Laribi-Habchi et al., 2020; Sahoo et al., 2024).

3.3. Characterization of purified chitinase enzyme

For the structural and morphological characterization of purified chitinase enzyme FTIR, SEM and TEM techniques were employed. In the analyses, characteristic structural peaks and morphological formations

Table 2
Purification steps of chitinase from *B. amyloliquefaciens* M6.

Enzyme fraction	Activity (U/mL) ± SD	Volume (mL)	Protein (mg/mL) ± SD	Total Protein (mg)	Total Activity (U)	Specific Activity (U/mg protein)	Purification fold	Yield (%)
Cell free extract	22.38 ± 0.3	250	1.04 ± 0.1	260	5595	21.52	1.00	100
$(NH_4)_2SO_4$	17.62 ± 0.2	15	0.52 ± 0.0	7.80	264.30	33.88	1.57	4.72
DEAE-Sephadex ion exchange chromatography	11.48 ± 0.0	9	0.05 ± 0.0	0.45	103.32	229.60	6.79	1.84

SD: Standard deviation.

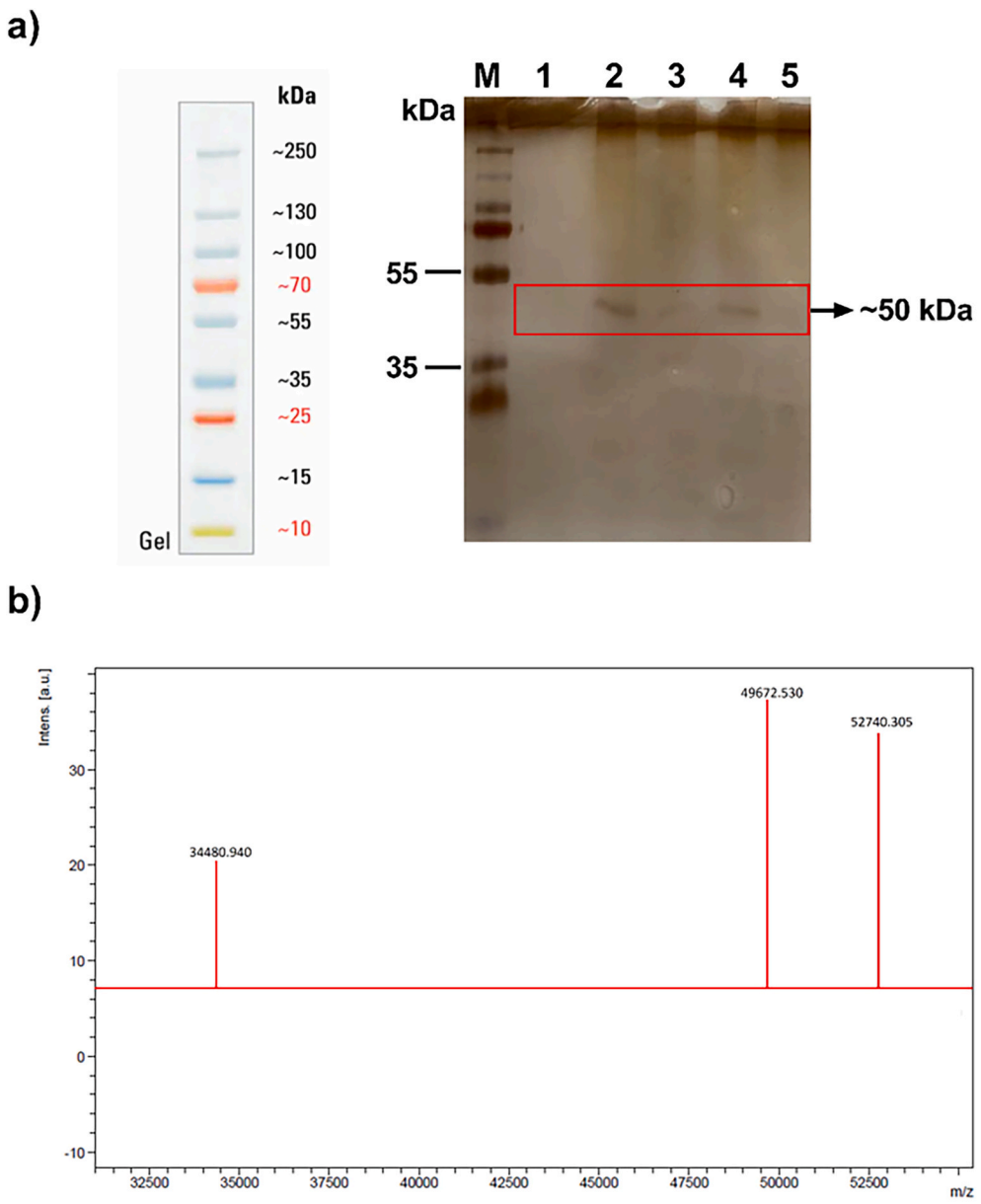


Fig. 3. SDS PAGE image of the purified enzyme **(a)**: **M:** Marker (Thermo scientific, catalog number: 26619), **1, 5:** No upload, **2, 3, 4**: Chitinase enzyme; MALDI-TOF-MS image **(b)**.

of the enzyme were examined. The broad peak observed at 3298 cm^{-1} in the FT-IR spectrum is attributed to the N-H bond stretching vibrations of the primary amine group in the enzyme structure (Fig. 4a). The peaks at 3082 and 2953 cm^{-1} were formed by the symmetric and asymmetric bond stretching vibrations of the CH_3 and CH_2 groups present in the chitinase structure, respectively. In addition, the peaks in the spectrum attributed to amide I at 1664 cm^{-1} and amide II linkages at 1541 cm^{-1}, and to the C-O bond stretching of the peptide bond at 1126 cm^{-1} support the successful obtaining of the pure enzyme structure.

SEM and TEM imaging were performed at different magnifications to determine the morphological properties of the purified chitinase enzyme. Although the recorded SEM image (Fig. 4b) showed the spherical morphology of the chitinase enzyme at some points, the enzyme mostly took on a bulk structure due to aggregation. Nevertheless, high magnification TEM images (Fig. 4c and d) clearly showed that the purified enzyme had a partially spherical morphological structure.

3.4. Structural and morphological characterization of ZnO/RGO NCs

The surface composition of ZnO/RGO NCs and the chemical states of elements were analyzed by XPS measurements. C 1s to determine the reduction of GO and Zn 2p and O 1s spectra recorded to determine the oxidation state of Zn element in the metal oxide structure are shown in Fig. 5a–c. The peak observed at 284.8 eV in the C 1s core spectrum (Fig. 5a) is attributed to the C-C bonds of RGO structure, while the two peaks observed at 286.4 eV and 288.6 eV are attributed to the C-O and C=O bonds, respectively (Rumble Jr et al., 1992). In the spectrum of ZnO/RGO NCs deconvolved according to the Gaussian function for the O 1s region (Fig. 5b), a peak at 530.0 eV was observed, which corresponds to the presence of the oxygen element in the form of metal oxide. Beside, the peak detected at 531.8 eV is attributed to the presence of C-O bonds. The photoelectrons detected at 1022 eV and 1045 eV in the Zn 2p core spectrum (Fig. 5c) are associated with the Zn 2p3/2 and Zn 2p1/2 valence states of ZnO, respectively. The binding energies in the core spectrum, which has a spin-orbit splitting of about 23 eV, are in good

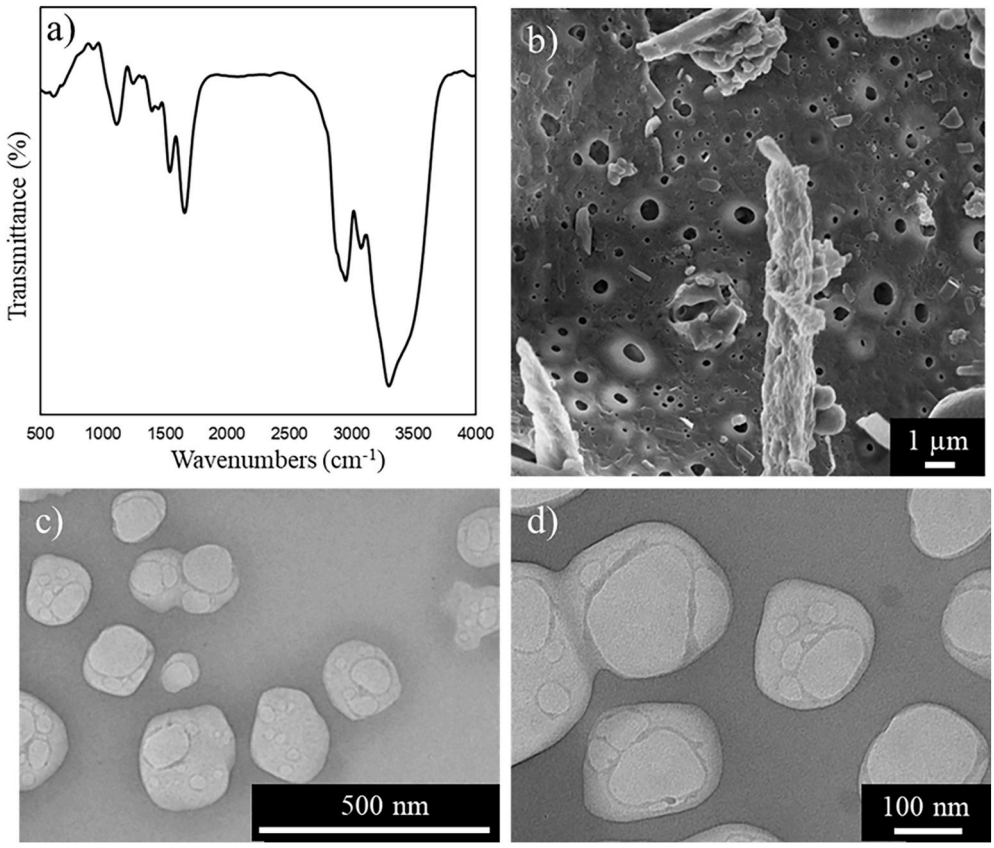


Fig. 4. FT-IR spectrum **(a)**, SEM image **(b)** and TEM images **(c, d)** of the purified chitinase enzyme.

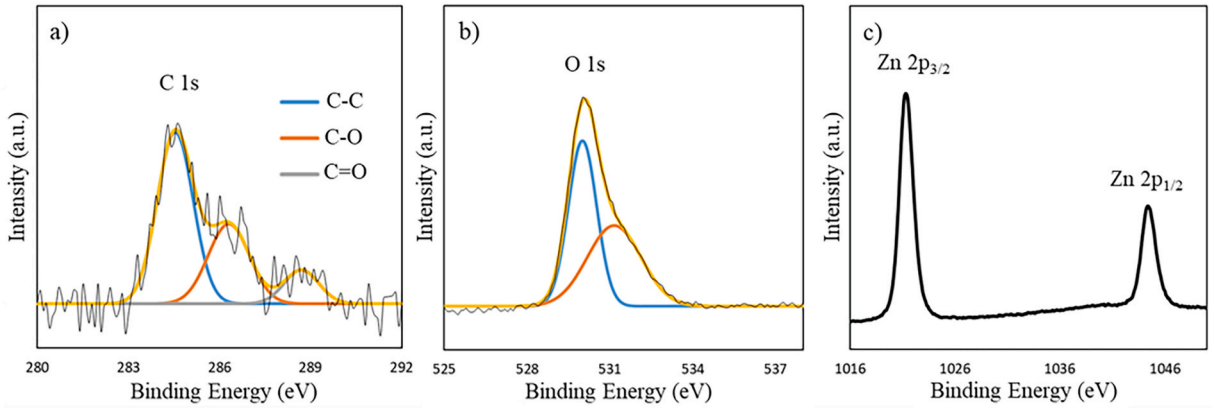


Fig. 5. C 1s **(a)**, O 1s **(b)**, and Zn 2p **(c)** XPS core spectra of ZnO/RGO NCs.

agreement with the values previously reported in the literature. XPS analysis showed that ZnO/RGO NCs could be synthesized in pure form using the green synthesis method, within the scope of the values obtained in accordance with the literature.

EDS analysis was performed to determine the elemental composition of ZnO/RGO NCs obtained using green synthesis. In the EDS spectrum given in Fig. S1a, no element other than C, O and Zn elements constituting the nanocomposite component is detected, supporting that ZnO/RGO NCs can be produced in pure elemental composition using green synthesis. We have also perform FT-IR to analyse the functional groups of ZnO/RGO. GO contains various functional groups such as –C-O, –OH, C-OH and -C=O in its structure. Green synthesis of ZnO/RGO also includes the reduction of these oxygenated groups by casting out from GO structure. The detailed analysis of FT-IR spectra is illustrated in Fig. S1b.

Raman scattering is a sensitive tool used to characterize the electronic structure of carbon material. Fig. 6a shows the Raman spectrum of ZnO/RGO prepared by green synthesis. For comparison purposes, Raman spectra of GO and green reduced RGO are also given in Fig. 6b. In the Raman spectrum, the vibration values of the G and D bands of GO observed at 1587 and 1341 cm^{-1}, respectively, are in good agreement with the wave numbers reported for the G and D bands of GO in the literatüre (Wilson et al., 2009). In the Raman spectrum of green reduced RGO, the G band, which provides information about the in-plane vibrations of sp^2 bonded carbon atoms, was observed at 1590 cm^{-1} and the D band, which is attributed to the presence of sp^3 defects in graphene, was observed at 1347 cm^{-1}. Similarly, the D band and G band were observed at 1585 and 1338 cm^{-1} in the ZnO/RGO structure. In this spectrum, similar to the green reduced RGO spectrum versus GO

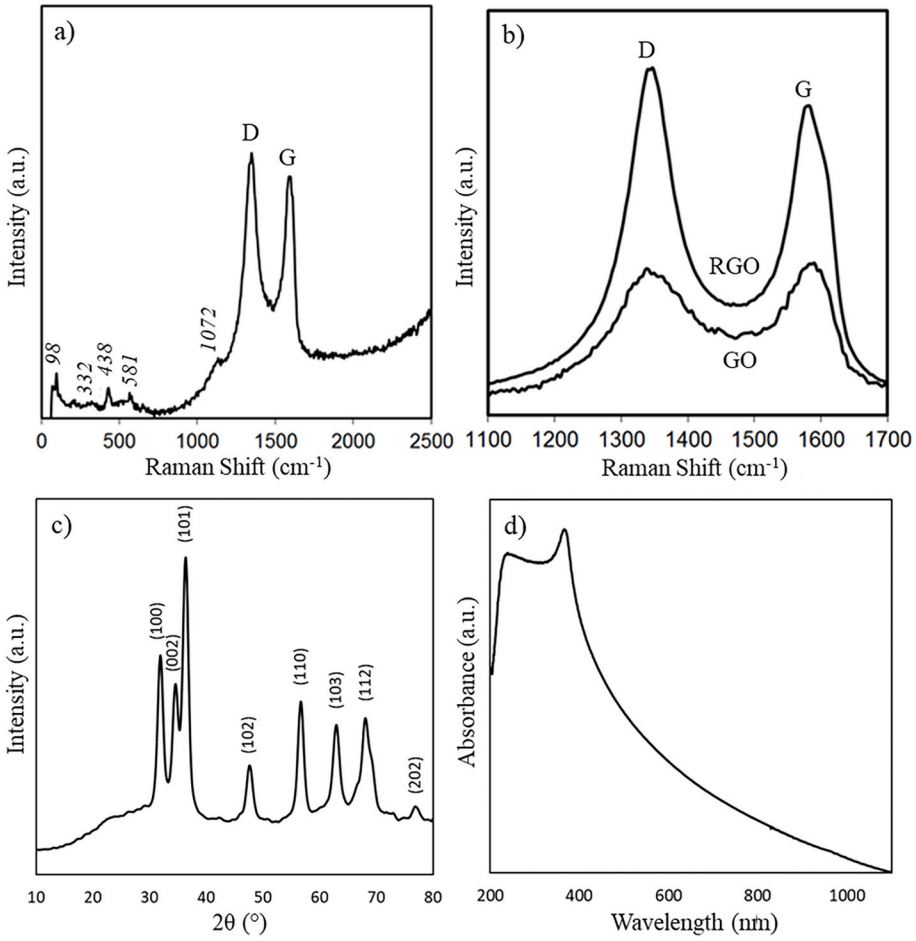


Fig. 6. Raman spectra of ZnO/RGO NCs **(a)**, GO and green reduced RGO **(b)**. XRD spectrum **(c)** and UV–VIS absorption spectrum **(b)** of ZnO/RGO NCs.

spectrum, it was observed that the peak intensity of the G band, which is related to the stacking shape of the graphene structure, decreased, and the peak intensity of the D band, which is related to the disorder of the system, increased. The ratio of D and G band intensities (I_D/I_G) of the nanocomposite (1.04) is larger than GO (0.91). Moreover, the peaks observed at low shifts at 98, 330, 438 and 581 cm^{-1} are the characteristic Raman peaks of ZnO with hexagonal wurtzite structure, which is associated with the multi-phonon scattering process (Zhou et al., 2012). The observed band shift, increase in D and G band ratio (I_D/I_G) and characteristic Raman peaks of ZnO in the results obtained from Raman spectroscopy support the successful production of ZnO/RGO NCs by the green synthesis method.

Crystallographic analysis was performed with the recorded XRD spectrum (Fig. 6c) for structural characterization of the ZnO/RGO NCs. The spectrum contains peaks at 2θ 31.8°, 34.5°, 36.3°, 47.5°, 56.7°, 62.9°, 67.9°, 72.5° and 76.8°, which are marked on the (100), (002), (101), (102), (110), (103), (112), (004) and (202) planes (JCPDS-36-1451) of ZnO, respectively (Kaur et al., 2019). The absence of any diffraction peak around $2\theta = 12.3°$ corresponding to the GO structure in the XRD spectrum supports that GO was successfully reduced by the green synthesis method. The absence of the $2\theta = 24.5°$ diffraction peak corresponding to the RGO structure in the diffractogram can be attributed to the disruption of the stacking order due to the composite of the RGO layers with ZnO Nps (Pan et al., 2012). XRD spectrum supports that ZnO/RGO NCs can be successfully grown in crystalline structure by the green synthesis method.

For the structural analysis of ZnO/RGO NCs, UV–VIS absorption spectrum (Fig. 6d) was examined to determine the absorption wavelength. The absorption peak occurring at approximately 240 nm wavelength in the spectrum is attributed to the π-π* transition of the aromatic C-C bonds in the RGO structure (Zhao et al., 2019). In the absorption spectrum, the absence of the peak at 310 nm corresponding to the n-π* transition of the carbonyl groups in the GO structure also supports the presence of RGO. Also, the presence of a peak at approximately 370 nm, which is attributed to the electronic transition of ZnO, was observed in the spectrum. The detection of this absorption peak compared to ZnO reported in the literature (388 nm) at lower wavelengths can be attributed to the fact that ZnO was obtained in nanoparticle form (Jay Chithra et al., 2015).

The morphological features of ZnO/RGO synthesized using green synthesis were elucidated by SEM and TEM images examined at different magnifications (Fig. 7a–d). The SEM image shown in Fig. 7a reveals the characteristic wrinkled layers of RGO. Besides, it is clearly seen that these crumpled-like layer surfaces are densely covered with ZnO nanoparticles. It was also observed in high magnification TEM images that the characteristic crumpled-like wrinkled layers of RGO were well composited with ZnO Nps (Fig. 7b). From the TEM images with higher magnification (Fig. 7c and d), it is determined that the ZnO/RGO has a nanostructural form and large surface area, which is important for its immobilization with chitinase enzyme. The morphological analyses prove both the good decoration of the ordered ZnO nanoparticles to the RGO layers to increase the surface area and the formation of 3D porous structures in the desired nanoparticle form for better enzyme activity.

3.5. Immobilization of chitinase on ZnO/RGO NCs

Adsorption and covalent linkage methods have recently become

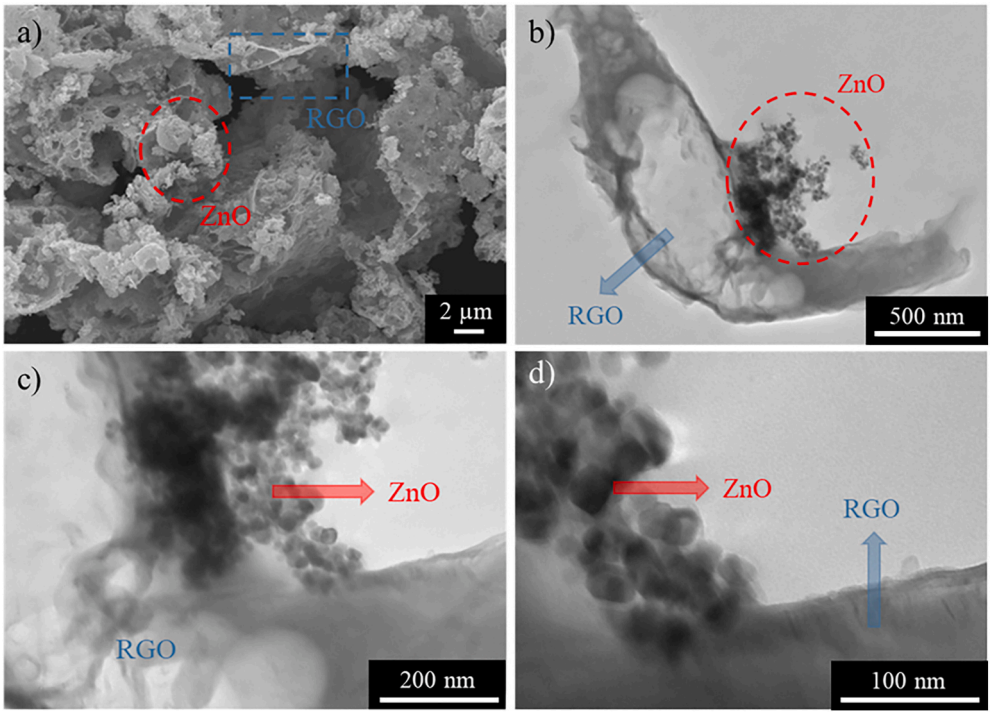


Fig. 7. SEM image **(a)** and TEM images **(b–d)** of ZnO/RGO NCs.

widely used in the immobilization of chitinase (Ismail et al., 2024; Charoenpol et al., 2024; Tawfiq et al., 2025). The combination of adsorption and glutaraldehyde cross-linking is a good option to prevent loss of adsorbed enzymes from the support and steric hindrance resulting from cross-linking. Adsorption can be used to preserve the catalytic activity of immobilized enzymes, while cross-linking can be used to maintain their stability (Qian et al., 2023). In the present study, chitinase was immobilized onto ZnO/RGO NCs first by adsorption and then by cross-linking. The effectiveness of immobilization was evaluated considering the recovered activity and immobilization efficiency results. Pre-immobilization free chitinase activity was measured as 11.48 U/mL, and post-immobilization activity was determined as 10.82 U/mL. Post-immobilization efficiency was calculated as 99.68 %, and recovered activity as 94.30 %. The results showed that the enzyme retained a significant portion of its activity and that the recovered activity was high. The yield and recovered activity are higher than the results of chitinase immobilized on magnetic nanoparticles, chitosan beads, and cellulose membranes in previous studies (Kidibule et al., 2021; Li and Mao, 2022; Charoenpol et al., 2024).

3.6. *Structural and morphological characterization of chitinase immobilized ZnO/RGO NCs*

For the structural characterization of chitinase immobilized ZnO/RGO, XPS, EDS, XRD, FT-IR, and Raman spectroscopy techniques were handled. We have also employed SEM and TEM analysis to describe the morphological effect of enzyme immobilization to ZnO/RGO NCs. The photoelectrons related to the bonds of chitinase immobilized nanocomposite were investigated by C 1s and O 1s core level XPS spectra. In the spectra detailed in Fig. S2a and b, the photoelectrons generated due to C-N bond and Zn-O, C-O bonds support enzyme immobilization and confirm the nanocomposite structure.

In the FTIR spectrum of chitinase-enzyme immobilized ZnO/RGO (Fig. 8a), the peak at 1128 cm^{-1} originating from C-O stretching vibrations of the peptide bond, the peak at 2943 cm^{-1} attributed to the asymmetric bond stretching vibration of CH_2 groups, the peak at 3196

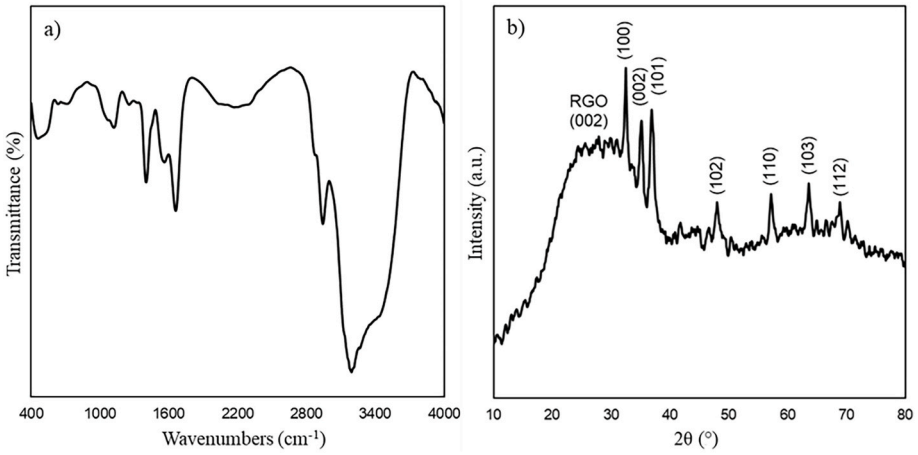


Fig. 8. FT-IR **(a)** and XRD **(b)** spectra of the chitinase immobilized ZnO/RGO NCs.

cm^{-1} wavenumber due to the stretching vibration in N-H bonds and the peaks at 1660 and 1533 cm^{-1} occurring from amide I and amide II groups, respectively, are observed. Additionally, the absorption band centered at ~500 cm^{-1} is attributed to the Zn-O bond vibration. When the FT-IR spectrum obtained for chitinase immobilized ZnO/RGO is compared with ZnO/RGO and purified chitinase enzyme, it is noticeable that each component preserves its characteristic structure except that the shifting of peak positions to lower wave numbers and decreasing intensities due to the chemical interaction between the functional groups of ZnO/RGO NCs and chitinase enzyme.

The XRD spectrum of chitinase enzyme immobilized ZnO/RGO NCs (Fig. 8b) contains diffraction peaks at 2θ 31.8°, 34.5°, 36.3°, 47.5°, 56.7°, 62.9° and 67.9° corresponding to the (100), (002), (101), (102), (110), (103) and (112) planes of the ZnO, respectively. The diffractogram also contains a broad band centered at ~25° corresponding to the (002) plane of the RGO structure. The presence of diffraction peaks corresponding to various crystal planes of RGO and ZnO, and the absence of any impurity peak indicate that the ZnO/RGO NCs retain their structural properties after the enzyme immobilization process.

EDS and Raman analyses for the structural characterization of the chitinase enzyme immobilized ZnO/RGO NCs are presented in detail Fig. S3a and b. The evidences obtained from the detailed analyses support the successful immobilization of the enzyme, and the formation of chitinase immobilized ZnO/RGO, purely.

SEM and TEM images recorded at different magnifications for the morphological analysis of chitinase enzyme immobilized ZnO/RGO were presented in Fig. 9a–d. SEM image shows that the surface of the chitinase enzyme, which takes on a bulk structure owing to aggregation, is mostly covered with ZnO/RGO in nanostructure form. SEM image shows that the surface of the chitinase enzyme, which takes on a bulk structure owing to aggregation, is mostly covered with nanostructured ZnO/RGO. In high magnification TEM image (Fig. 9b), it is seen that the chitinase enzyme largely preserves its partially spherical morphological structure, does not undergo any morphological deformation, and integrates with the characteristic crumpled-like wrinkled layer of RGO. Furthermore, higher magnification TEM images (Fig. 9c and d) clearly reveal the interaction of the chitinase enzyme surface with the ZnO particles in nanoparticle form, supporting the successful immobilization of ZnO/RGO NCs with chitinase enzyme. The observed morphology of the immobilized enzyme with nanostructured Zno/RGO indicates a high enzyme activity due to its large surface area.

3.7. *Effect of temperature and pH on the activity of free and immobilized chitinase*

Determining the optimum pH and temperature of enzymes is very important for high activity and efficient enzyme production (Devi et al., 2023). To determine the optimum reaction temperature of the purified chitinase, enzyme activity was measured at different temperatures (15–85) and the optimum temperature was determined as 45 °C (Fig. 10a). Enzyme activity increased with a gradual increase in temperature and decreased sharply when the temperature exceeded 45 °C. Similar results were reported for chitinases purified from *Streptomyces mutabilis* IMA8 (45 °C), *B. velezensis* (44 °C), *B. amyloliquefaciens* V656 (40 °C), *B. cereus* NK91 (40 °C) and *Aeromonas* sp. CQNU6-2 (40 °C) (Wang et al., 2002; Ma et al., 2021; Thakur et al., 2022a; Dahiya et al., 2022; Rajendran et al., 2024). In addition, many studies have reported that the optimum temperature value of bacterial chitinases is in the range of 40–60 °C (Malik et al., 2023; Aktas et al., 2023). In addition, there are several thermostable chitinases isolated from different sources has been reported previously (Hungund et al., 2022; Gilvanova et al., 2022).

Most of the chitinases identified to date have shown optimal activity at acidic or near neutral pH (Essghaier et al., 2021; Thakur et al., 2022a; Ezzine et al., 2024). In parallel with literature studies, the purified chitinase showed its optimum activity at pH 6 and its activity decreased at lower/higher pHs (Fig. 10b). Similar results were obtained from chitinases purified from *B. amyloliquefaciens* V656 (pH 6), *B. licheniformis* B307 (pH 6), *B. paralicheniformis* HL37 (pH 6), *B. haynesii* (pH 6) (Wang et al., 2002; Farooq et al., 2021; Govindaraj et al., 2024; Ma et al., 2024). In contrast to the results obtained, there are chitinases showing optimum activity in alkaline conditions (Kim et al., 2021; Lv

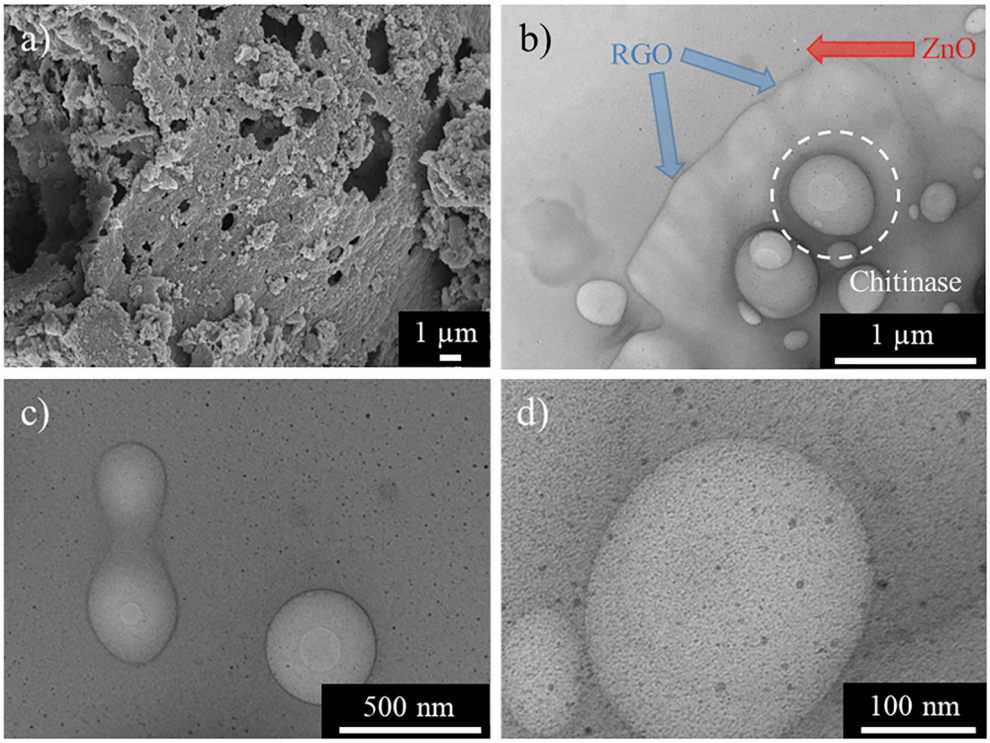


Fig. 9. SEM image **(a)** and TEM images **(b–d)** of the chitinase immobilized ZnO/RGO NCs.

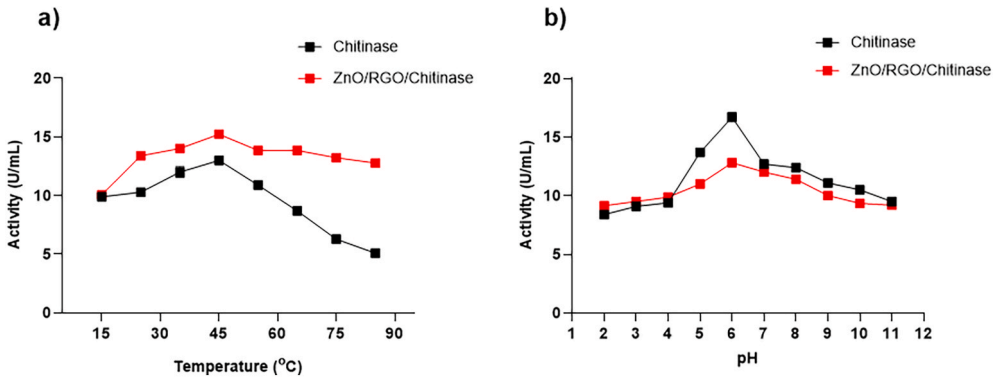


Fig. 10. (a) Effect of temperature on free and immobilized chitinase activity (Error bars are not visible because the standard error values are too low); **(b)** Effect of pH on free and immobilized chitinase activity (Error bars are not visible because the standard error values are too low).

et al., 2021). Immobilized chitinase was not much affected by changing temperature and pH values compared to free chitinase and remained more stable (Fig. 10a and b). The immobilized chitinase retained most of its activity over a wide range of temperatures (35–65 °C) and pH (4.0–9.0), reaching optimum activity at pH 6 and 45 °C. Similarly, it has been reported by many researchers that immobilized enzymes are more stable and stable at varying temperatures and pH values compared to their free forms (Kidibule et al., 2021; Charoenpol et al., 2024).

3.8. Insecticidal activity of immobilized chitinase

The insecticidal activity of nanobioformulation was tested against important storage pests *R. dominica* and *O. surinamensis*. Corrected mortality rates were obtained by applying Abbott (1987) formula to the number of dead insects obtained after the treatment (Tables 3 and 4). In *R. dominica* species, the median mortality rates differed statistically according to the treatments and a significant difference was found between the control (water) treatment and 6 mg/mL (109.2 U/mL) nanobioformulation dose and deltamethrin treatment ($p < 0.001$) (Table 3). While mortality rate was 0 % in the control treatment, it was 100 % in the other two treatments. In *O. surinamensis*, the highest mortality rate (100 %) was achieved at nanobioformulation doses of 10 mg/mL (182.0 U/mL) and 12 mg/mL (218.4 U/mL) and with deltamethrin treatment, but the median mortality rates did not differ statistically ($p > 0.050$) (Table 3). ZnO/RGO NC, used in chitinase immobilization, was applied as a control against both pests, and mortality rates were determined as 50.7 % and 33.3 % for *R. dominica* and *O. surinamensis*, respectively. In addition, the lethal effect of the free chitinase enzyme on pests (mortality rates of 81.3 % for *R. dominica* and 92.0 % for *O. surinamensis*) was much higher than that of the nanocomposite. The increased activity of chitinase after immobilization may be attributed to the combined effect with the nanocomposite and the increased stability of the enzyme. Indeed, the insecticidal activity of ZnO and RGO NCs has been reported in previous studies (Ali et al., 2025, Lampiri et al., 2024).

The probit analysis for *R. dominica* and *O. surinamensis* species was conducted to determine the effect of different doses and number of days on insect mortality (Table 4). The result showed that the dose variable had a statistically significant effect on the number of dead insects ($p < 0.001$). LC_{50} (the concentration that causes the death of 50 % of insects after treatment) and LC_{90} (the concentration that causes the death of 90 % of insects after treatment) values of the nanobioformulation for *R. dominica* were as 1.8 mg/mL (32.8 U/mL) and 3.8 mg/mL (69.2 U/mL), respectively, and for *O. surinamensis* were 4.8 mg/mL (87.4 U/mL) and 10.0 mg/mL (182.0 U/mL), respectively (Table 4). According to the results of the analysis, the day variable was found to be positive and statistically significant for both insect species ($p < 0.001$) (Table 5). This result shows that the probability of death increases with the passage of time. The LT_{50} (time it takes for 50 % of insects to mortality) for the 6 mg/mL (109.2 U/mL) treatment with the highest mortality rate (100 %) in *R. dominica* was approximately 1.43 days and LT_{90} (time it takes for 90 % of insects to mortality) was approximately 5.95 days, LT_{50} for deltamethrin was approximately 0.15 days and LT_{90} was approximately 0.64 days, LT_{50} for chitinase treatment was approximately 4.60 days and LT_{90} was approximately 19.17 days (Table 5). In *O. surinamensis*, the highest mortality rate (100 %) was reached for 10 mg/mL (182.0 U/mL) and 12 mg/mL (218.4 U/mL) treatments, LT_{50} and LT_{90} were determined as 1.58 and 2.07 days, respectively, and 7.89 and 10.36 days, respectively (Table 5). For deltamethrin, LT_{50} was approximately 0.27 days and LT_{90} was approximately 1.34 days; for chitinase treatment, LT_{50} was approximately 4.07 days and LT_{90} was approximately 20.36 days. In parallel with our findings, numerous studies have emphasized the efficacy of chitinase and chitinase-producing microorganisms against agricultural pests (Rajendran et al., 2024; Wu et al., 2025; Dikbaş et al., 2025). For example, Mahmood et al. (2020) applied *Xenorhabdus nematophila* chitinase to *Helicoverpa armigera* larvae and reported severe mortality in larvae after feeding. Similarly, chitinase purified from *B. cereus* C-13 was tested against *Helopeltis theivora* and the enzyme was reported to cause 78 % mortality (Suganthi et al., 2020). In addition, Dikbaş et al. (2021) tested ZnO Np immobilized chitinase enzyme against *Sitophilus zeamais* and obtained a 100 % mortality rate. Again, chitinase ChiB was tested against *Spodoptera frugiperda* and high mortality rates were observed (El-Sayed et al., 2024). In addition, oral administration of *Trichoderma asperellum* chitinase to *Bombyx mori* larvae negatively affected their survival and development (Berini et al., 2024).

3.8.1. Morphologic observations

The insect cuticle and the hairs in the cuticle are a complex and important body part that is essential for the survival of all insects (Sugumaran, 2022). Loss of these structures can impair the insect's ability to sense its environment or regulate its body temperature, leading to its death (Rabadiya and Behr, 2024). In order to observe the damage caused by nanobioformulation on the insect cuticle, the elytra of dead insects taken from the doses with the highest mortality rate (6 mg/mL (109.2 U/mL) for *R. dominica*, 10 mg/mL (182.0 U/mL) for *O. surinamensis*) were observed using SEM device and the images obtained are presented in Fig. 11. SEM analysis provided clear visualisations of the destructive effects of chitinase on the insect cuticle and showed that the hairs in the elytra of nanobioformulated insects were shed, the hair holes disappeared and the integrity of the cuticle layer started to deteriorate compared to the elytra of control insects (Fig. 11). In addition to the cuticle layer, the digestive systems of the treated insects were examined under a microscope and it was observed that there was a very small amount of food residues in the digestive systems of the adult insects (Fig. 12), while there were more food residues in the

Table 3
Insecticidal activity of the treatments against *R. dominica* and *O. surinamensis*.

Insect	Application	Mortality Rate (%)		p
		Mean (%) ± SD	Median (%) (min - max)[a]	
R. dominica	0.5 mg/mL (9.1 U/mL)	6.7 ± 2.3	8.0 (4.0–8.0)^{ab}	**<0.001**
	1 mg/mL (18.2 U/mL)	20.0 ± 4.0	20.0 (16.0–24.0)^{ab}	
	1.5 mg/mL (27.3 U/mL)	25.3 ± 2.3	240 (24.0–28.0)^{ab}	
	2 mg/mL (36.4 U/mL)	44.0 ± 4.0	44.0 (40.0–48.0)^{ab}	
	4 mg/mL (72.8 U/mL)	97.3 ± 2.3	96.0 (96.0–100.0)^{ab}	
	6 mg/mL (109.2 U/mL)	100.0 ± 0.0	100.0 (100.0–100.0)^{b}	
	Deltamethrin	100.0 ± 0.0	100.0 (100.0–100.0)^{b}	
	Chitinase	81.3 ± 20.1	84.0 (60.0–100.0)^{ab}	
	RGO	38.7 ± 6.1	40.0 (32.0–44.0)^{ab}	
	Control (Water)	0.0 ± 0.0	0.0 (0.0–0.0)^{a}	
	ZnO Np	50.7 ± 6.1	52.0 (44.0–56.0)^{ab}	
	ZnO/RGO NCs	50.7 ± 6.1	52.0 (44.0–56.0)^{ab}	
	Total	51.2 ± 35.4	44.0 (0.0–100.0)^{ab}	
O. surinamensis	2 mg/mL (36.4 U/mL)	10.7 ± 4.6	8.0 (8.0–16.0)	**0.003**
	4 mg/mL (72.8 U/mL)	30.7 ± 6.1	32.0 (24.0–36.0)	
	6 mg/mL (109.2 U/mL)	66.7 ± 57.7	100.0 (0.0–100.0)	
	8 mg/mL (145.6 U/mL)	65.3 ± 34.0	64.0 (32.0–100.0)	
	10 mg/mL (182.0 U/mL)	100.0 ± 0.0	100.0 (100.0–100,0)	
	12 mg/mL (218.4 U/mL)	100.0 ± 0.0	100.0 (100.0–100.0)	
	Deltamethrin	100.0 ± 0.0	100.0 (100.0–100.0)	
	Chitinase	92.0 ± 13.9	100.0 (76.0–100.0)	
	RGO	6.7 ± 6.1	8.0 (0.0–12.0)	
	Control (Water)	0.0 ± 0.0	0.0 (0.0–0.0)	
	ZnO Np	33.3 ± 2.3	32.0 (32.0–36.0)	
	ZnO/RGO NCs	33.3 ± 8.3	36.0 (24.0–40.0)	
	Total	53.2 ± 41.1	36.0 (0.0–100.0)	

[a] Kruskal Wallis test, a-b: There is no difference between groups with the same letter.

digestive system of the insects in the control group compared to the treated insects. Similarly, Aktas et al. (2023) reported that after 5-day treatment of *Leptinotarsa decemlineata* with chitinase, the head and legs of the insects were detached and the tight structures of the hexagonal cells on the elytra surface were disrupted. Additionally, Tawfiq et al. (2025) reported that treatment with chitinase/Co-MOF caused significant morphological changes around the head of *Tribolium castaneum*, damage to the elytra, and ultimately death.

3.8.2. Intestinal enzyme profile

The effect of nanobioformulation on three enzymes (ALP, LDH, ATPase) important in insect metabolism was determined by comparing the intestinal enzyme activities of insects taken from the dose with the highest mortality rate and control treatment. ALP activity was 22.3 U/mL, LDH activity was 17.3 U/mL and ATPase activity was 31.8 U/mL at 6 mg/mL (109.7 U/mL) nanobioformulation dose, which caused the highest mortality in *R. dominica* (Fig. 13). In the control treatment of the species, ALP, LDH and ATPase activities were determined as 30.4 U/mL, 71.0 U/mL and 70.9 U/mL, respectively. When ALP, LDH and ATPase activities were considered, a significant difference was observed between nanobioformulation and control treatment ($p < 0.05$, $p < 0.0001$). ALP activity was measured as 10.6 U/mL, LDH activity as 29.7 U/mL and ATPase activity as 68.3 U/mL at 10 mg/mL (182.0 U/mL) nanobioformulation dose, which caused the highest mortality in *O. surinamensis* (Fig. 13). In the control treatment of this species, ALP, LDH and ATPase activities were determined as 16.4 U/mL, 34.3 U/mL and 125.8 U/mL, respectively. When ALP, LDH and ATPase activities were considered, the difference between nanobioformulation and control treatment for each enzyme was very significant ($p < 0.05$, $p < 0.001$, $p < 0.0001$). The results showed that the LDH, ALP and ATPase activities of *R. dominica* and *O. surinamensis* fed with nanobiophomulated diet were lower compared to control insects. This may be due to the toxic effects of chitinase application on insect metabolism and peritrophic membrane (Chandrasekaran et al., 2014; Dikbaş et al., 2023). Indeed, Chandrasekaran et al. (2014) reported that LHD and ATPase activity decreased in *Spodoptera litura* larvae fed a diet containing chitinase. Similarly, Dikbaş et al. (2023) reported that immobilized chitinase application on ZnO NPs decreased the LDH, ALP and ATPase activity of *S. zeamais*. In addition, it has been reported that some fungi and mycotoxins, different plant extracts and oils are used for biocontrol purposes and the activities of related enzymes decrease significantly after application (Shahriari et al., 2020; Datta et al., 2021; Soliman et al., 2022; Madasamy et al., 2023). Literature data and findings show that chitinase application affects the detoxification and metabolic enzymes of insects and causes enzyme inhibition

Table 5
Effect of nanobioformulation doses on the lifespan of *R. dominica* and *O. surinamensis* adults.

Insect	Application	LT_{50} (d) (95 % CL)	LT_{90} (d) (95 % CL)
R. dominica	6 mg/mL (109.2 U/mL)	1.4 (1.1–1.9)	6.0 (4.6–7.8)
	Deltamethrin	0.2 (0.1–0.5)	0.6 (0.1–2.0)
	Chitinase	4.6 (3.8–5.8)	19.2 (15.2–25.1)
O. surinamensis	10 mg/mL (182.0 U/mL)	1.6 (1.0–2.4)	7.9 (5.0–13.3)
	12 mg/mL (218.4 U/mL)	2.1 (1.4–3.0)	10.4 (6.9–16.9)
	Deltamethrin	0.3 (0.1–0.8)	1.34 (0.5–3.9)
	Chitinase	4.1 (3.2–5.1)	20.36 (15.6–28.4)

LT_{50}: Time it takes for 50 % of insects to mortality, LT_{90}: Time it takes for 90 % of insects to mortality, d: day, CL: confidence limits.

Table 4
Lethal concentrations (LC_{50} and LC_{90}) of nanobioformulation against *R. dominica* and *O. surinamensis* adults.

Insect	LC_{50} (mg/mL) (95 % CL)	LC_{50} (U/mL) (95 % CL)	LC_{90} (mg/mL) (95 % CL)	LC_{90} (U/mL) (95 % CL)
R. dominica	1.8 (1.5–2.2)	32.8 (27.3–40.0)	3.8 (2.9–5.6)	69.2 (52.8–101.9)
O. surinamensis	4.8 (3.9–5.8)	87.4 (71.0–105.6)	10.0 (8.0–13.6)	182.0 (145.6–247.5)

LC_{50}: The concentration that causes the death of 50 % of insects after treatment, LC_{90}: The concentration that causes the death of 90 % of insects after treatment, CL: confidence limits.

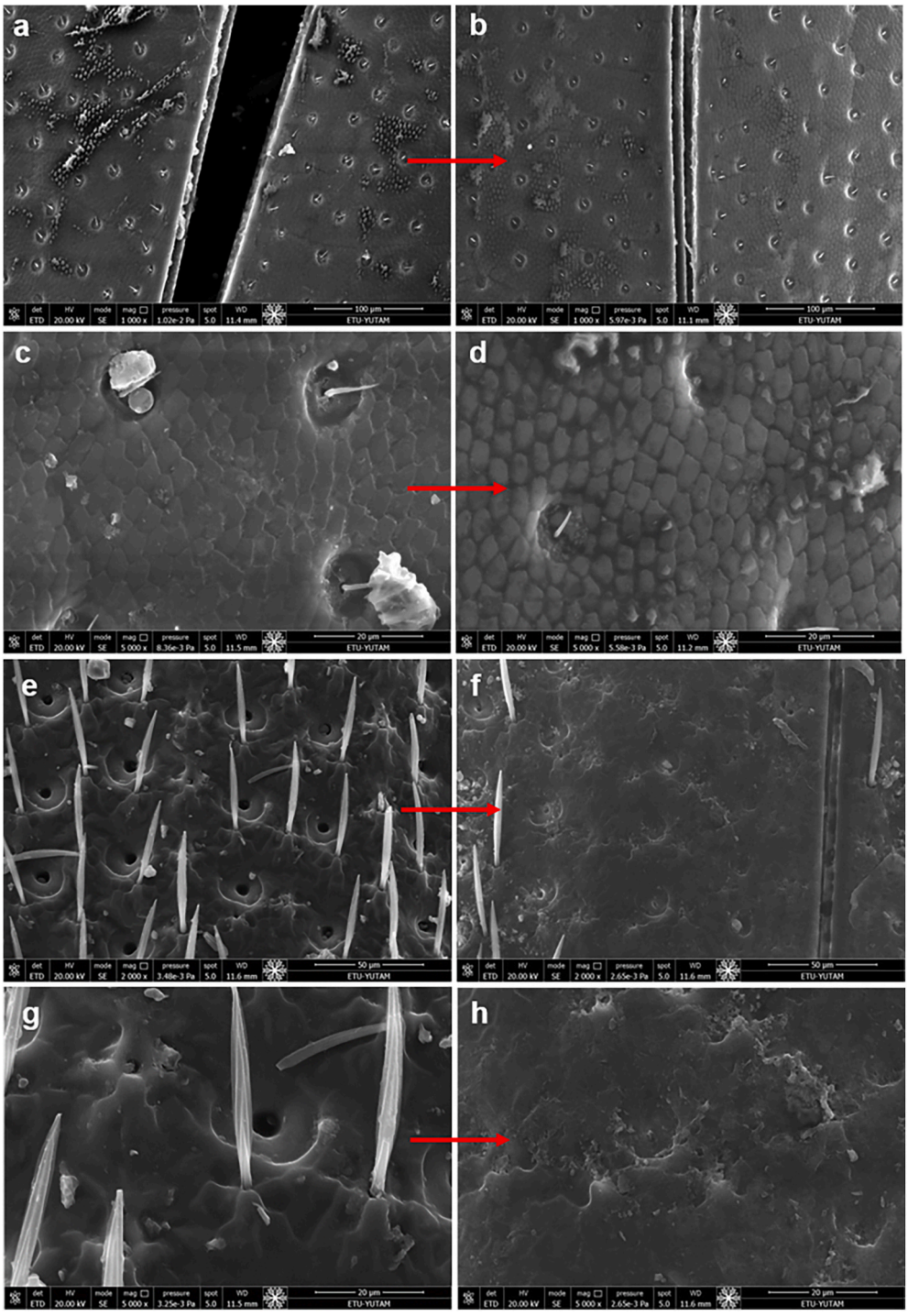


Fig. 11. *R. dominica* and *O. surinamensis* under scanning electron microscopy (50 μm and 20 μm), **(a)** Elytra (50 μm) of untreated (Control) *R. dominica*, **(b)** Elytra (50 μm) of treated *R. dominica*, **(c)** Elytra (20 μm) of untreated (Control) *R. dominica,* **(d)** Elytra (20 μm) of treated *R. dominica*, **(e)** Elytra (50 μm) of untreated (Control) *O. surinamensis*, **(f)** Elytra (50 μm) of treated *O. surinamensis*, **(g)** Elytra (20 μm) of untreated (Control) *O. surinamensis*, **(h)** Elytra (20 μm) of treated *O. surinamensis*.

(Chandrasekaran et al., 2014; Dikbaş et al., 2023).

4. Conclusion

The results of the study determined that *B. amyloliquefaciens* M6 produced optimum chitinase under mesophilic and slightly acidic conditions, achieving maximum chitinase enzyme production within a relatively short incubation period of 24 h. Both free and and immobilized chitinase purified from this strain showed optimum activity in acidic pH (6.0) and mesophilic temperature (45 °C). Notably, the immobilized enzyme revealed greater stability than the free enzyme under changing temperature and pH conditions. In addition, the nanobioformulation (immobilized chitinase) showed high insecticidial activity against *R. dominica* and *O. surinamensis*. Given the adverse environmental and health impacts associated with chemical pesticides, the application of environmentally friendly biocontrol strategies that are biodegradable, safe for human health, and capable of providing prolonged efficacy represents a promising alternative within the framework

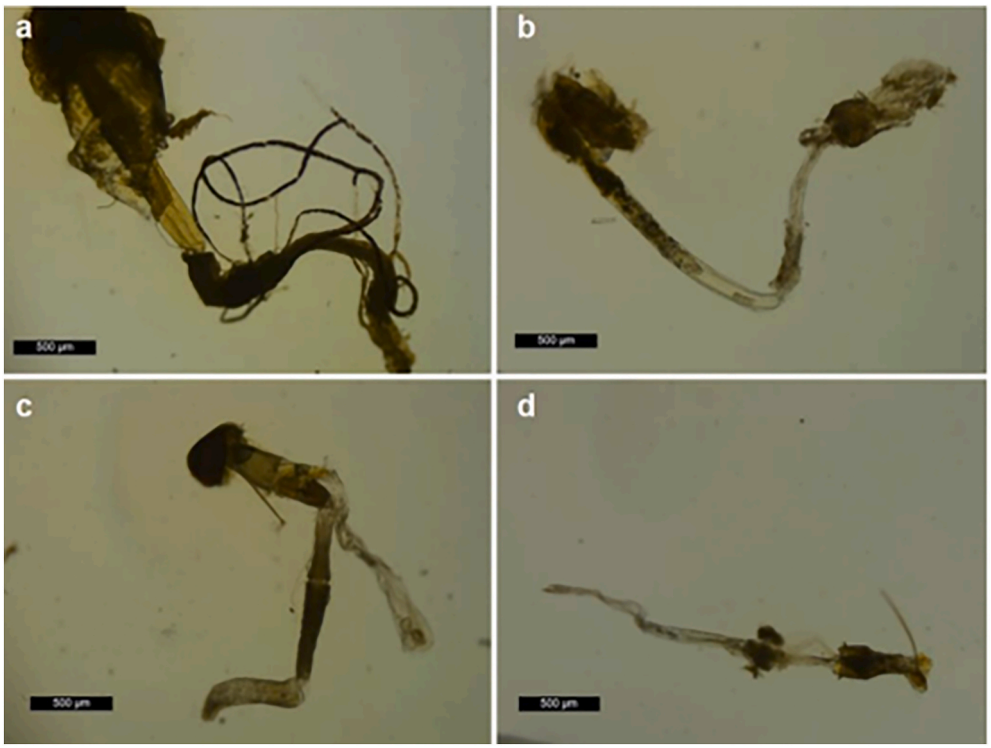


Fig. 12. Image of insect intestines under a stereo microscope, (**a)** Untreated (control) *R. dominica*, **(b)** Treated *R. dominica*, (**c)** Untreated (control) *O. Surinamensis,* **(d)** Treated *O. surinamensis*.

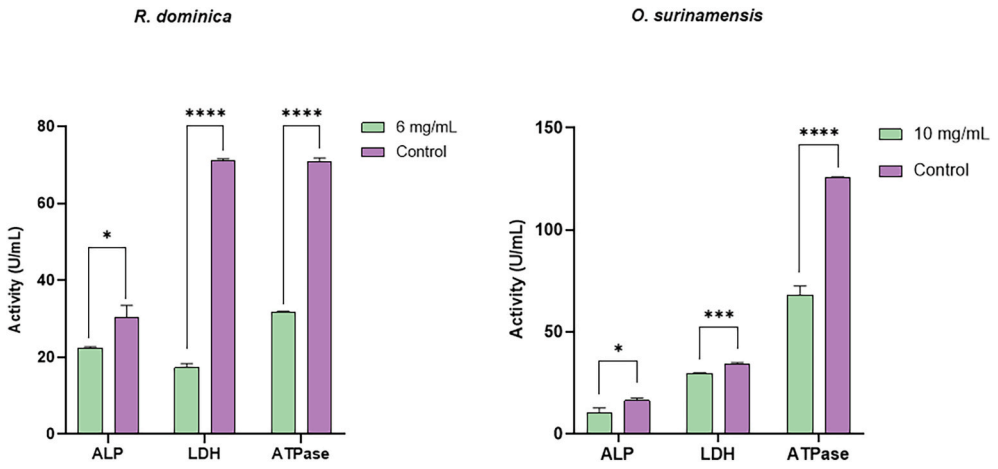


Fig. 13. ALP, LDH and ATPase activities of *R. dominica* and *O. surinamensis* according to treatments (*: $p < 0.05$, ***:$p < 0.001$, ****:$p < 0.0001$).

of sustainable agriculture. Future studies should focus on evaluating the long-term effectiveness of the nanobioformulation and assessing the influence of storage conditions on its stability and performance.

CRediT authorship contribution statement

Neslihan Dikbaş: Conceptualization, Project administration, Funding acquisition, Writing - Original Draft
Sevda Uçar: Conceptualization, Methodology, Visualization, Writing - Original Draft
Şeyma Alım: Methodology, Writing - Review & Editing
Emir Çepni: Visualization, Methodology, Writing - Review & Editing
Göksel Tozlu: Methodology, Writing- Reviewing and Editing
Merve Şenol Kotan: Methodology, Writing- Reviewing and Editing
Tuba Öznülüer Özer: Visualization, Writing- Reviewing and Editing
Muhammed Tatar: Methodology, Writing- Reviewing and Editing
Kağan Kökten: Writing- Reviewing and Editing
Tolga Karaköy: Writing- Reviewing and Editing
Barış Binay: Writing- Reviewing and Editing

Funding

This study was supported by the Scientific and Technological Research Council of Türkiye (TUBITAK) (Grant Number: 122O387) and Atatürk University Scientific Research Projects (BAP) Coordination Unit (Grant Number: FDA-2023-12952).

Declaration of competing interest

The authors declare the following financial interests/personal

relationships which may be considered as potential competing interests: Neslihan Dikbas reports financial support was provided by Scientific and Technological Research Council of Türkiye. Neslihan Dikbas reports financial support was provided by Ataturk University. If there are other authors, they declare that they have no known competing financial interests or personal relationships that could have appeared to influence the work reported in this paper.

Acknowledgments

The authors would like to thank the Scientific and Technological Research Council of Turkey (TUBITAK) and Atatürk University Scientific Research Projects Coordination Unit.for financial support. The authors thank Dr. Amjad Ali for reviewing and improving the English language of the manuscript.

Appendix A. Supplementary data

Supplementary data to this article can be found online at https://doi.org/10.1016/j.jspr.2026.102958.

Data availability

All data relevant to the article are included in the article.

References

Aasim, M., Ali, A., Ulaş, F., Tatar, M., Liaqat, W., Altaf, M.T., Rahimi, M., 2025. Myconanoparticles: a sustainable strategy for agricultural applications and phytopathogen management. Beni-Suef University Journal of Basic and Applied Sciences 14 (1), 123. https://doi.org/10.1186/s43088-025-00713-y.

Abbott, W.S., 1987. A method of computing the effectiveness of an insecticide. J. Am. Mosq. Control Assoc. 3 (2), 302–303.

Altammar, K.A., 2023. A review on nanoparticles: characteristics, synthesis, applications, and challenges. Front. Microbiol. 14, 1155622. https://doi.org/10.3389/fmicb.2023.1155622.

Abirami, S., Yogalsakshmi, K., Pushpa, A.S.R., Kananan, M., 2016. Screening and identification of chitin degrading bacteria from shrimp shell waste dumping soil environment and its media optimization for chitinase enzyme production. World J. Pharm. Pharmaceut. Sci. 5 (11), 743–757. https://doi.org/10.20959/wjpps201611-7713.

Adetiloye, O.A., Solomon, B.O., Omolaiye, J.A., Betiku, E., 2025. Optimization of thermostable amylolytic enzyme production from *Bacillus cereus* isolated from a recreational warm spring via Box Behnken design and response surface methodology. Microb. Cell Fact. 24 (1), 87. https://doi.org/10.1186/s12934-025-02709-w.

Ahamed, M., Akhtar, M.J., Khan, M.M., Alhadlaq, H.A., 2022. Facile green synthesis of ZnO-RGO nanocomposites with enhanced anticancer efficacy. Methods 199, 28–36. https://doi.org/10.1016/j.ymeth.2021.04.020.

Ahmed, S., Ashraf, M., Yousaf, S., Alsafari, I.A., Akhtar, M., Shahid, M., Somaily, H.H., Warsi, M.F., 2023. High-performance, non-enzymatic glucose sensor based on Fe and Cu doped ZnO/rGO based nanocomposite. Mater. Chem. Phys. 297, 127335. https://doi.org/10.1016/j.matchemphys.2023.127335.

Akeed, Y., Atrash, F., Naffaa, W., 2020. Partial purification and characterization of chitinase produced by *Bacillus licheniformis* B307. Heliyon 6 (5), 127335. https://doi.org/10.1016/j.heliyon.2020.e03858.

Aktas, C., Ruzgar, D., Gurkok, S., Gormez, A., 2023. Purification and characterization of *Stenotrophomonas maltophilia* chitinase with antifungal and insecticidal properties. Prep. Biochem. Biotechnol. 53 (7), 797–806. https://doi.org/10.1080/10826068.2022.2142942.

Aktuganov, G.E., Safina, V.R., Galimzianova, N.F., Gilvanova, E.A., Kuzmina, L.Y., Melentiev, A.I., Baymiev, A.H., Lopatin, S.A., 2022. Constitutive chitosanase from *Bacillus thuringiensis* B-387 and its potential for preparation of antimicrobial chitooligomers. World J. Microbiol. Biotechnol. 38 (10), 167. https://doi.org/10.1007/s11274-022-03359-5.

Ali, A., Chand, K., Liu, C., Hassan, A., Hassan, H., Liu, X., Lu, M., 2025. Insecticidal and antibacterial properties of zinc oxide nanoparticles (ZnO-NPs) synthesized from Phoebe zhennan leaf extract. J. Asia Pac. Entomol., 102474 https://doi.org/10.1016/j.aspen.2025.102474.

Alsafran, M., Razavi, M.M., Rizwan, M., Usman, K., 2025. A review on synthesis and characterization of selenium nanoparticles from plant extracts for applications in agriculture, biomedicine, and environment. Green Chem. Lett. Rev. 18 (1), 2488237. https://doi.org/10.1080/17518253.2025.2488237.

General Directorate of Agricultural Research and Policies (GDARP), 2024. Plant Pests Standard Pesticide Trial Methods. https://www.tarimorman.gov.tr/TAGEM/Belgeler/yayin/Ambar%20Zararl%C4%B1lar%C4%B1%20Standart%20%C4%B0la%C3%A7%20Deneme%20Metotlar%C4%B1.pdf (accessed February 2024).

Aparna, S.M., Rakhi, R.B., 2025. A non-enzymatic electrochemical sensor based on zinc oxide/reduced graphene oxide (ZnO/rGO) nanocomposite for effective detection of urea. Mater. Sci. Eng., B 312, 117862. https://doi.org/10.1016/j.mseb.2024.117862.

Berini, F., Montali, A., Liguori, R., Venturini, G., Bonelli, M., Shaltiel-Harpaz, L., Reguzzoni, M., Siti, M., Marinelli, F., Casartelli, M., Tettamanti, G., 2024. Production and characterization of *Trichoderma asperellum* chitinases and their use in synergy with *Bacillus thuringiensis* for lepidopteran control. Pest Manag. Sci. 80 (7), 3401–3411. https://doi.org/10.1002/ps.8045.

Bhattacharya, S., Das, A., Samadder, S., Rajan, S.S., 2016. Biosynthesis and characterization of a thermostable, alkali-tolerant chitinase from *Bacillus pumilus* JUBCH08 displaying antagonism against phytopathogenic *Fusarium oxysporum*. 3 Biotech 6 (1), 87. https://doi.org/10.1007/s13205-016-0406-x.

Bradford, M.M., 1976. A rapid and sensitive method for the quantitation of microgram quantities of protein utilizing the principle of protein-dye binding. Anal. Biochem. 72 (1–2), 248–254.

Brzezinska, M.S., Kalwasińska, A., Świątczak, J., Żero, K., Jankiewicz, U., 2020. Exploring the properties of chitinolytic *Bacillus* isolates for the pathogens biological control. Microb. Pathog. 148, 104462. https://doi.org/10.1016/j.micpath.2020.104462.

Cahyaningtyas, H.A.A., Suyotha, W., Cheirsilp, B., Yano, S., 2021. Statistical optimization of halophilic chitosanase and protease production by *Bacillus cereus* HMRSC30 isolated from *Terasi* simultaneous with chitin extraction from shrimp shell waste. Biocatal. Agric. Biotechnol. 31, 101918. https://doi.org/10.1016/j.bcab.2021.101918.

Chaiharn, M., Pikomol, A., Lumyoung, S., 2019. Purification and characterization of an extracellular chitinase from *Bacillus thuringiensis* R 176 using solid state fermentation with shrimp shells waste. Chiang Mai J. Sci. 46, 495–509.

Chandrasekaran, R., Revathi, K., Thanigaivel, A., Kirubakaran, S.A., Senthil-Nathan, S., 2014. *Bacillus subtilis* chitinase identified by matrix-assisted laser desorption/ionization time-of flight/time of flight mass spectrometry has insecticidal activity against *Spodoptera litura* Fab. Pestic. Biochem. Physiol. 116, 1–12. https://doi.org/10.1016/j.pestbp.2014.09.013.

Charoenpol, A., Crespy, D., Schulte, A., Suginta, W., 2024. Immobilized chitinase as effective biocatalytic platform for producing bioactive di-N-acetyl chitobiose from recycled chitin food waste. Bioresour. Technol. 406, 130945. https://doi.org/10.1016/j.biortech.2024.130945.

Dahiya, D., Pilli, A., Chirra, P.R.R., Sreeramula, V., Mogili, N.V., Ayothiraman, S., 2022. Morphological and structural characterization of chitin as a substrate for the screening, production, and molecular characterization of chitinase by *Bacillus velezensis*. Environ. Sci. Pollut. Control Ser. 29 (57), 86550–86561. https://doi.org/10.1007/s11356-022-22166-x.

Das, M.P., Rebecca, L.J., Sharmila, S., Barman, A., Dhiraj, K., 2012. Identification and optimization of cultural conditions for chitinase production by *Bacillus amyloliquefaciens* SM3. J. Chem. Pharmaceut. Res. 4 (11), 4816–4821.

Datta, R., Kaur, A., Saraf, I., Singh, I.P., Kaur, S., 2021. Enzymatic suppression activity of *Alpinia galanga* extract against polyphagous lepidopteran pest *Spodoptera litura* (Fabricius). Arch. Phytopathol. Plant Protect. 54 (19–20), 1807–1821. https://doi.org/10.1080/03235408.2021.1943805.

de Sousa, I.G., Oliveira, J., Mexia, A., Barros, G., Almeida, C., Brazinha, C., Vega, A., Brites, C., 2023. Advances in environmentally friendly techniques and circular economy approaches for insect infestation management in stored rice grains. Foods 12 (3), 511. https://doi.org/10.3390/foods12030511.

Deeba, F., Shakir, H.A., Irfan, M., Khan, M., Qazi, J.I., 2022. Utilization of agro-industrial waste for chitinase production by locally isolated *Bacillus subtilis* using response surface methodology. Pakistan J. Zool. 54, 551–560. https://doi.org/10.17582/journal.pjz/20190717070735.

del Arco, L., Riudavets, J., Castañé, C., 2024. *Cephalonomia tarsalis* (Hymenoptera: Bethylidae) for the control of the sawtoothed grain beetle, either alone or in combination with the predatory mite *Blattisocius tarsalis*. J. Stored Prod. Res. 105, 102250. https://doi.org/10.1016/j.jspr.2024.102250.

Devi, S., Chauhan, A., Bishist, R., Sankhyan, N., Rana, K., Sharma, N., 2023. Production, partial purification and efficacy of keratinase from *Bacillus halotolerans* L2EN1 isolated from the poultry farm of Himachal Pradesh as a potential laundry additive. Biocatal. Biotransform. 41 (3), 222–242. https://doi.org/10.1080/10242422.2022.2029851.

Dikbaş, N., Tülek, A., Uçar, S., Alım, Ş., Servili, B., Paçal, N., Tozlu, G., Ercisli, S., 2025. Biocontrol potential of *Vibrio maritimus* chitinase: heterologous expression and insecticidal activity against *Acanthoscelides obtectus*. Int. J. Biol. Macromol., 144285 https://doi.org/10.1016/j.ijbiomac.2025.144285.

Dikbaş, N., Ucar, S., Tozlu, G., Özer, T.Ö., Kotan, R., 2023. The effect of immobilized chitinase enzyme on the biocontrol of *Sitophilus zeamais*. Turk. J. Agric. For. 47 (2), 170–177. https://doi.org/10.55730/1300-011X.3075.

Dikbaş, N., Uçar, S., Tozlu, G., Öznülüer Özer, T., Kotan, R., 2021. Bacterial chitinase biochemical properties, immobilization on zinc oxide (ZnO) nanoparticle and its effect on *Sitophilus zeamais* as a potential insecticide. World J. Microbiol. Biotechnol. 37 (10), 173. https://doi.org/10.1007/s11274-021-03138-8.

Dukariya, G., Kumar, A., 2020. Chitinase production from locally isolated *Bacillus cereus* GS02 from chitinous waste enriched soil. Journal of Advances in Biology & Biotechnology 23, 39–48. https://doi.org/10.9734/JABB/2020/v23i130137.

Dukariya, G., Kumar, A., 2021. Statistical optimization of chitinase production by Box-Behnken design in submerged fermentation using *Bacillus cereus* GS02. J. Appl. Biol. Biotechnol. 9 (2), 60–66. https://doi.org/10.7324/JABB.2021.9205.

El Aalaoui, M., Rammali, S., Kamal, F.Z., Bencharki, B., Ciobică, A., Hogas, M., Novac, B., Sbaghi, M., 2025. Biocontrol of *Cassida vittata* Vill. (Coleoptera: chrysomelidae) in

sugar beet crops using *Streptomyces* sp. strains. Microbiol. Res. 16 (3), 57. https://doi.org/10.3390/microbiolres16030057.
El-Sayed, G.M., Emam, M.T., Hammad, M.A., Mahmoud, S.H., 2024. Gene cloning, heterologous expression, and in silico analysis of chitinase B from *Serratia marcescens* for biocontrol of *Spodoptera frugiperda* larvae infesting maize crops. Molecules 29 (7), 1466. https://doi.org/10.3390/molecules29071466.
Essghaier, B., Zouaoui, M., Najjari, A., Sadfi, N., 2021. Potentialities and characterization of an antifungal chitinase produced by a halotolerant *Bacillus licheniformis*. Curr. Microbiol. 78 (2), 513–521. https://doi.org/10.1007/s00284-020-02329-0.
Ezzine, A., Ben Hadj Mohamed, S., Bezzine, S., Aoudi, Y., Hajlaoui, M.R., Baciou, L., Smaali, I., 2024. Improved expression of a thermostable GH18 bacterial Chitinase in two different *Escherichia coli* strains and its potential use in plant protection and biocontrol of Phytopathogenic Fungi. Mol. Biotechnol. 66 (9), 2635–2647. https://doi.org/10.1007/s12033-023-01041-1.
Farooq, M.A., Ali, S., Hassan, A., Tahir, H.M., Mumtaz, S., Mumtaz, S., 2021. Biosynthesis and industrial applications of α-amylase: a review. Arch. Microbiol. 203 (4), 1281–1292. https://doi.org/10.1007/s00203-020-02128-y.
Gilvanova, E.A., Aktuganov, G.E., Safina, V.R., Milman, P.Y., Lopatin, S.A., Melentiev, A. I., Galimzianova, N.F., Kuzmina, L.Y., Boyko, T.F., 2022. Characterization of thermotolerant chitinase from the strain *Cohnella* sp. IB P-192 and its application for the production of bioactive chitosan oligomers. Appl. Biochem. Microbiol. 58 (2), 143–154. https://doi.org/10.1134/S0003683822020077.
Govindaraj, V., Anandan, D.K., Kim, S.K., Raval, R., Raval, K., 2025. Process optimisation for improved chitinase production from marine isolate *Bacillus haynesii* and bioethanol production with *Saccharomyces cerevisiae*. Braz. J. Microbiol. 1–16. https://doi.org/10.1007/s42770-025-01644-7.
Govindaraj, V., Kim, S.K., Raval, R., Raval, K., 2024. Marine *Bacillus haynesii* chitinase: purification, characterization and antifungal potential for sustainable chitin bioconversion. Carbohydr. Res. 541, 109170. https://doi.org/10.1016/j.carres.2024.109170.
Gupta, N., Kumar, A., Laksh, S.A., Rana, M., 2017. Process optimization of extracellular chitinase production from *Bacillus* sp. isolated from fish waste Dumping site. European Journal of Pharmaceutical and Medical Research 4, 474–480.
Harvinda, Y., Ustadi, U., Putra, M.M.P., 2023. Production, purification and characterization of chitinase from *Micromonospora* sp. AR17. Indonesian Journal of Biotechnology 28 (1), 46–55. https://doi.org/10.22146/ijbiotech.77137.
Hashem, A.S., Guedes, R.N.C., Awadalla, H.S., 2021. Feeding substrate and temperature interplay determining infestations and losses by the sawtoothed grain beetle (*Oryzaephilus surinamensis*). J. Stored Prod. Res. 94, 101887. https://doi.org/10.1016/j.jspr.2021.101887.
Hassan, M.W., Sarwar, G., Farooqi, M.A., Jamil, M., 2021. Extent and pattern of damage in wheat caused by three different species of storage insect pests. Int. J. Trop. Insect Sci. 41 (1), 593–599. https://doi.org/10.1007/s42690-020-00246-0.
Hassanisaadi, M., Barani, M., Rahdar, A., Heidary, M., Thysiadou, A., Kyzas, G.Z., 2022. Role of agrochemical-based nanomaterials in plants: biotic and abiotic stress with germination improvement of seeds. Plant Growth Regul. 97 (2), 375–418. https://doi.org/10.1007/s10725-021-00782-w.
Hazare, C., Bhagwat, P., Singh, N.K., Singh, S., Pillai, S., 2025. Statistical optimization and kinetic modeling simulation for fibrinolytic enzyme production by *Bacillus tropicus* from mahewu, a traditional South African fermented food. Process Biochem. 153, 122–134. https://doi.org/10.1016/j.procbio.2025.03.010.
Huang, S., Huang, H., Xie, J., Wang, F., Fan, S., Yang, M., Zheng, C., Han, L., Zhang, D., 2022. The latest research progress on the prevention of storage pests by natural products: species, mechanisms, and sources of inspiration. Arab. J. Chem. 15 (11), 104189. https://doi.org/10.1016/j.arabjc.2022.104189.
Hungund, B.S., Tennalli, G.B., Achappa, S., Divate, M.N., 2022. Production and partial purification of thermostable chitinase from *Bacillus cereus* BSH-4 and its antifungal activity. J. Biochem. Technol. 13 (2–2022), 46–53. https://doi.org/10.51847/RAlF1H5BCe.
Ismail, S.A., Fayed, B., Abdelhameed, R.M., Hassan, A.A., 2024. Chitinase-functionalized UiO-66 framework nanoparticles active against multidrug-resistant *Candida Auris*. BMC Microbiol. 24 (1), 269. https://doi.org/10.1186/s12866-024-03414-1.
Jamil, Z., Mukhtar, T., Raja, M.U., Shahbaz, M., Seelan, J.S.S., Tatar, M., Usanmaz, B.A., 2025. Utilization of phytogenic silver nanoparticles and bacterial agents for the management of citrus canker disease. Turk. J. Agric. For. 49 (6), 998–1008. https://doi.org/10.55730/1300-011X.3319.
Jay Chithra, M., Sathya, M., Pushpanathan, K.J.A.M.S., 2015. Effect of pH on crystal size and photoluminescence property of ZnO nanoparticles prepared by chemical precipitation method. Acta Metall. Sin. 28 (3), 394–404. https://doi.org/10.1007/s40195-015-0218-8.
Kaur, P., Rani, S., Lal, B., 2019. Excitation dependent photoluminescence properties of ZnO nanophosphor. Optik 192, 162929. https://doi.org/10.1016/j.ijleo.2019.162929.
Kaur, R., Choudhary, D., Bali, S., Bandral, S.S., Singh, V., Ahmad, M.A., Rani, N., Singh, T.G., Chandrasekaran, B., 2024. Pesticides: an alarming detrimental to health and environment. Sci. Total Environ. 915, 170113. https://doi.org/10.1016/j.scitotenv.2024.170113.
Khalid, A., Ali, S., Rukhma, Jahangeer, M., Sarwar, A., Nelofer, R., Aziz, T., Alharbi, M., Alasmari, A.F., Albekairi, T.H., 2023. Immobilization of *Aspergillus oryzae* tyrosine hydroxylase on ZnO nanocrystals for improved stability and catalytic efficiency towards L-dopa production. Sci. Rep. 13 (1), 22882. https://doi.org/10.1038/s41598-023-50198-x.
Kidibule, P.E., Costa, J., Atrei, A., Plou, F.J., Fernandez-Lobato, M., Pogni, R., 2021. Production and characterization of chitooligosaccharides by the fungal chitinase Chit42 immobilized on magnetic nanoparticles and chitosan beads: selectivity, specificity and improved operational utility. RSC Adv. 11 (10), 5529–5536. https://doi.org/10.1039/D0RA10409D.
Kim, S.K., Park, J.E., Oh, J.M., Kim, H., 2021. Molecular characterization of four alkaline chitinases from three chitinolytic bacteria isolated from a mudflat. Int. J. Mol. Sci. 22 (23), 12822. https://doi.org/10.3390/ijms222312822.
Krolicka, M., Hinz, S.W., Koetsier, M.J., Joosten, R., Eggink, G., van den Broek, L.A., Boeriu, C.G., 2018. Chitinase Chi1 from *Myceliophthora thermophila* C1, a thermostable enzyme for chitin and chitosan depolymerization. J. Agric. Food Chem. 66 (7), 1658–1669. https://doi.org/10.1021/acs.jafc.7b04032.
Kumar, D., 2012. Identification and optimization of cultural conditions for chitinase production by *Bacillus amyloliquefaciens* SM3. J. Chem. Pharmaceut. Res. 4 (11), 4816–4821.
Lampiri, E., Yap, P.L., Berillis, P., Athanassiou, C.G., Losic, D., 2024. Graphene powders as new contact nanopesticides: revealing key parameters on their insecticidal activity for stored product insects. Chemosphere 364, 143200. https://doi.org/10.1016/j.chemosphere.2024.143200.
Laribi-Habchi, H., Bouacem, K., Allala, F., Jabeur, F., Selama, O., Mechri, S., Yahiaoui, M., Bouanane-Darenfed, A., Jaouadi, B., 2020. Characterization of chitinase from *Shewanella inventionis* HE3 with bio-insecticidal effect against granary weevil, *Sitophilus granarius* Linnaeus (Coleoptera: *curculionidae*). Process Biochem. 97, 222–233. https://doi.org/10.1016/j.procbio.2020.06.023.
Li, J., Mao, X., 2022. Construction of an immobilized enzyme membrane reactor for efficient and sustainable conversion of ionic liquid/ultrasound-pretreated chitin. ACS Sustain. Chem. Eng. 10 (23), 7536–7544. https://doi.org/10.1021/acssuschemeng.2c00792.
Los, A., Ziuzina, D., Boehm, D., Bourke, P., 2020. Effects of cold plasma on wheat grain microbiome and antimicrobial efficacy against challenge pathogens and their resistance. Int. J. Food Microbiol. 335, 108889. https://doi.org/10.1016/j.ijfoodmicro.2020.108889.
Lv, C., Gu, T., Ma, R., Yao, W., Huang, Y., Gu, J., Zhao, G., 2021. Biochemical characterization of a GH19 chitinase from *Streptomyces alfalfae* and its applications in crystalline chitin conversion and biocontrol. Int. J. Biol. Macromol. 167, 193–201. https://doi.org/10.1016/j.ijbiomac.2020.11.178.
Ma, X., Zou, D., Ji, A., Jiang, C., Zhao, Z., Ding, X., Han, Z., Bao, P., Chen, K., Ma, A., Wei, X., 2024. Identification of a novel chitinase from *Bacillus paralicheniformis*: gene mining, sequence analysis, and enzymatic characterization. Foods 13 (11), 1777. https://doi.org/10.3390/foods13111777.
Ma, Z., Tong, J., Wang, Y., Zhou, Z., 2021. Isolation and characterization of a thermostable alkaline chitinase-producing *Aeromonas* strain and its potential in biodegradation of shrimp shell wastes. RomIan Biotechnol Lett 26 (2), 2511–2522. https://doi.org/10.25083/rbl/26.2/2511.2522.
Madasamy, M., Sahayaraj, K., Sayed, S.M., Al-Shuraym, L.A., Selvaraj, P., El-Arnaouty, S. A., Madasamy, K., 2023. Insecticidal mechanism of botanical crude extracts and their silver nanoliquids on *Phenacoccus solenopsis*. Toxics 11 (4), 305. https://doi.org/10.3390/toxics11040305.
Mahmood, S., Kumar, M., Kumari, P., Mahapatro, G.K., Banerjee, N., Sarin, N.B., 2020. Novel insecticidal chitinase from the insect pathogen *Xenorhabdus nematophila*. Int. J. Biol. Macromol. 159, 394–401. https://doi.org/10.1016/j.ijbiomac.2020.05.078.
Malik, M.S., Rehman, A., Khan, I.U., Khan, T.A., Jamil, M., Rha, E.S., Anees, M., 2023. Thermo-neutrophilic cellulases and chitinases characterized from a novel putative antifungal biocontrol agent: *bacillus subtilis* TD11. PLoS One 18 (1), e0281102. https://doi.org/10.1371/journal.pone.0281102.
Miller, G.L., 1959. Use of dinitrosalicylic acid reagent for determination of reducing sugar. Anal. Chem. 31 (3), 426–428.
Mir, S.A., Dar, B.N., Shah, M.A., Sofi, S.A., Hamdani, A.M., Oliveira, C.A., Moosavi, M.H., Khaneghah, A.M., Sant'Ana, A.S., 2021. Application of new technologies in decontamination of mycotoxins in cereal grains: challenges, and perspectives. Food Chem. Toxicol. 148, 111976. https://doi.org/10.1016/j.fct.2021.111976.
Mohammed, A.F., 2020. Optimization of cellulase and chitinase enzymes production by plant growth promoting rhizobacteria. Nov. Res. Microbiol. J. 4 (1), 641–652.
Ngegba, P.M., Cui, G., Khalid, M.Z., Zhong, G., 2022. Use of botanical pesticides in agriculture as an alternative to synthetic pesticides. Agriculture 12 (5), 600. https://doi.org/10.3390/agriculture12050600.
Ong, L.G., Lam, H.K., Lim, M.Y., Tan, T.X., 2017. Process optimization on chitinase production by locally isolated *Enterobacter* sp. and *Zymomonas* sp. International Journal of Chemical Engineering and Applications 8 (4), 286–289. https://doi.org/10.18178/ijcea.2017.8.4.671.
Pan, X., Zhao, Y., Liu, S., Korzeniewski, C.L., Wang, S., Fan, Z., 2012. Comparing graphene-TiO_2 nanowire and graphene-TiO_2 nanoparticle composite photocatalysts. ACS Appl. Mater. Interfaces 4 (8), 3944–3950. https://doi.org/10.1021/am300772t.
Pekdemir, S.S., Bakar, B., Taş, R., Ulu, A., Pekdemir, M.E., Ateş, B., 2024. Immobilization of Xylanase on ZnO nanoparticles obtained by green synthesis from *Eupatorium cannabinum* L. and its application in enrichment of fruit juices. Mol. Catal. 562, 114232. https://doi.org/10.1016/j.mcat.2024.114232.
Philip, N.V., Koteshwara, A., Kiran, G.A., Raja, S., Subrahmanyam, V.M., Chandrashekar, H.R., 2020. Statistical optimization for coproduction of chitinase and beta 1, 4-endoglucanase by chitinolytic *Paenibacillus elgii* PB1 having antifungal activity. Appl. Biochem. Biotechnol. 191 (1), 135–150. https://doi.org/10.1007/s12010-020-03235-8.
Poria, V., Rana, A., Kumari, A., Grewal, J., Pranaw, K., Singh, S., 2021. Current perspectives on chitinolytic enzymes and their agro-industrial applications. Biology 10 (12), 1319. https://doi.org/10.3390/biology10121319.
Priyadarshi, N., Singhal, N.K., 2025. Methods, applications, and challenges of enzyme immobilization on nanomaterials. Enzyme Immobilization with Nanomaterials: Applications and Challenges 1–28. https://doi.org/10.1021/bk-2025-1508.ch001.

Qian, J., Huang, A., Zhu, H., Ding, J., Zhang, W., Chen, Y., 2023. Immobilization of lipase on silica nanoparticles by adsorption followed by glutaraldehyde cross-linking. Bioproc. Biosyst. Eng. 46 (1), 25–38. https://doi.org/10.1007/s00449-022-02810-z.

Rabadiya, D., Behr, M., 2024. The biology of insect chitinases and their roles at chitinous cuticles. Insect Biochem. Mol. Biol. 165, 104071. https://doi.org/10.1016/j.ibmb.2024.104071.

Rajendran, K., Krishnamoorthy, M., Karuppiah, K., Ethiraj, K., Sekar, S., 2024. Chitinase from *Streptomyces mutabilis* as an effective eco-friendly biocontrol agent. Appl. Biochem. Biotechnol. 196 (1), 18–31. https://doi.org/10.1007/s12010-023-04489-8.

Rumble Jr, J.R., Bickham, D.M., Powell, C.J., 1992. The NIST x-ray photoelectron spectroscopy database. Surf. Interface Anal. 19 (1-12), 241–246. https://doi.org/10.1002/sia.740190147.

Sabbour, M., 2020. Effect of some essential oils on *Rhyzopertha dominica* (Coleoptera: bostrichidae). Int. Res. J. Biol. Sci. 2 (1), 32–37.

Sadi, S., Ghollasi, M., Eskandari, K., Darvishi, E., 2025. Innovative approaches in invertase immobilization: utilizing green synthesized zinc oxide nanoparticles to improve biochemical properties. Anal. Biochem. 696, 115661. https://doi.org/10.1016/j.ab.2024.115661.

Sahoo, S., Badhe, M.R., Paul, A., Sahoo, P.K., Suryawanshi, A.R., Panda, D., Pillai, B.R., Baliarsingh, S., Patnaik, B.B., Mohanty, J., 2024. Isolation and characterization of a lectin-like chitinase from the hepatopancreas of freshwater prawn, *Macrobrachium rosenbergii*. Biochimie 221, 125–136. https://doi.org/10.1016/j.biochi.2023.09.025.

Sasi, A., Duraipandiyan, N., Marikani, K., Dhanasekaran, S., Al-Dayan, N., Venugopal, D., 2020. Identification and characterization of a newly isolated chitinase-producing strain *Bacillus licheniformis* SSCL-10 for chitin degradation. Archaea 2020 (1), 8844811. https://doi.org/10.1155/2020/8844811.

Senol, M., Nadaroglu, H., Dikbas, N., Kotan, R., 2014. Purification of Chitinase enzymes from *Bacillus subtilis* bacteria TV-125, investigation of kinetic properties and antifungal activity against *Fusarium culmorum*. Ann. Clin. Microbiol. Antimicrob. 13 (1), 35. https://doi.org/10.1186/s12941-014-0035-3.

Shahriari, M., Zibaee, A., Shamakhi, L., Sahebzadeh, N., Naseri, D., Hoda, H., 2020. Bio-efficacy and physiological effects of *Eucalyptus globulus* and *Allium sativum* essential oils against *Ephestia kuehniella* Zeller (Lepidoptera: pyralidae). Toxin Rev. 422–433. https://doi.org/10.1080/15569543.2018.1554588.

Singh, R.V., Singh, B., Kumar, A., Sambyal, K., Karuppanan, K.K., Lee, J.K., 2025. Enzyme immobilization on nanomaterials and their applications. Materials 18 (17), 4106. https://doi.org/10.3390/ma18174106.

Sirohi, R., Tarafdar, A., Gaur, V.K., Singh, S., Sindhu, R., Rajasekharan, R., Madhavan, A., Binod, P., Kumar, S., Pandey, A., 2021. Technologies for disinfection of food grains: advances and way forward. Food Res. Int. 145, 110396. https://doi.org/10.1016/j.foodres.2021.110396.

Soliman, A., Nada, M., Gad, A., 2022. Evaluation the effects of the entomopathogenic fungus *Beauveria bassiana* (Ascomycota: hypocrales) on some histological and physiological parameters for the green bug *Nezara viridula* (L.)(Hemiptera: pentatomidae). Alexandria Science Exchange Journal 43 (2), 229–238. https://doi.org/10.21608/asejaiqjsae.2022.239209.

Sudha, S., 2020. Optimization of chitinase production from lake sediment inhabitant *Bacillus thuringiensis* strain LS1 and *Bacillus cereus* strain LS2. Asian J. Pharm. 14 (2). https://doi.org/10.22377/ajp.v14i2.3611.

Suganthi, M., Arvinth, S., Senthilkumar, P., 2020. Comparative bioefficacy of Bacillus and Pseudomonas chitinase against *Helopeltis theivora* in tea (*Camellia sinensis* (L.) O. Kuntze. Physiol. Mol. Biol. Plants 26 (10), 2053–2060. https://doi.org/10.1007/s12298-020-00875-2.

Sugumaran, M., 2022. Cuticular sclerotization in insects–a critical review. Adv. Insect Physiol 62, 111–214. https://doi.org/10.1016/bs.aiip.2022.02.001.

Swathy, K., Parmar, M.K., Vivekanandhan, P., 2024. Biocontrol efficacy of entomopathogenic fungi *Beauveria bassiana* conidia against agricultural insect pests. Environ. Qual. Manag. 34 (1), e22174. https://doi.org/10.1002/tqem.22174.

Tawfiq, F.M., Abd El, F.E.Z.A., Salem, S.H., Elshahawy, A.M., Sayed, A.M., Abdel-Hafez, A.A., 2025. Enhanced biological activity of chitinase immobilized on cobalt metal-organic framework: isolation, characterization, and potential applications. Int. J. Biol. Macromol. 308, 142538. https://doi.org/10.1016/j.ijbiomac.2025.142538.

Thakur, N., Nath, A.K., Chauhan, A., Gupta, R., 2022. Purification, characterization, and antifungal activity of *Bacillus cereus* strain NK91 chitinase from rhizospheric soil samples of Himachal Pradesh, India. Biotechnol. Appl. Biochem. 69 (5), 1830–1842. https://doi.org/10.1002/bab.2250.

Tudi, M., Daniel Ruan, H., Wang, L., Lyu, J., Sadler, R., Connell, D., Chu, C., Phung, D.T., 2021. Agriculture development, pesticide application and its impact on the environment. Int. J. Environ. Res. Publ. Health 18 (3), 1112. https://doi.org/10.3390/ijerph18031112.

Tülek, A., 2025. Entrapment of *Geobacillus kaustophilus* lipase in ZIF-8 and cross-linking with genipin for biodiesel production from vegetable oils. Mol. Catal. 576, 114919. https://doi.org/10.1016/j.mcat.2025.114919.

Tülek, A., Şükür, G., Özdemir, F.İ., Varan, N.E., Yildirim, D., 2025. Immobilization of L-asparaginase on genipin and divinyl sulfone cross-linked multi-walled carbon nanotubes and silica supports for acrylamide mitigation. Food Chem., 145268 https://doi.org/10.1016/j.foodchem.2025.145268.

Tülek, A., Yıldırım, D., Aydın, D., Binay, B., 2021. Highly-stable *Madurella mycetomatis* laccase immobilized in silica-coated ZIF-8 nanocomposites for environmentally friendly cotton bleaching process. Colloids Surf. B Biointerfaces 202, 111672. https://doi.org/10.1016/j.colsurfb.2021.111672.

Wang, S.L., Shih, I.L., Liang, T.W., Wang, C.H., 2002. Purification and characterization of two antifungal chitinases extracellularly produced by *Bacillus amyloliquefaciens* V656 in a shrimp and crab shell powder medium. J. Agric. Food Chem. 50 (8), 2241–2248. https://doi.org/10.1021/jf010885d.

Wilson, N.R., Pandey, P.A., Beanland, R., Young, R.J., Kinloch, I.A., Gong, L., Liu, Z., Suenaga, K., Rourke, J.P., York, S.J., Sloan, J., 2009. Graphene oxide: structural analysis and application as a highly transparent support for electron microscopy. ACS Nano 3 (9), 2547–2556. https://doi.org/10.1021/nn900694t.

Wu, W., Chen, N., Hu, J., Zhang, J., Wu, Y., Yao, T., Wang, X., 2025. Function of chitinase in *Penicillium ochrochloron* Q-3-1 and its insecticidal and antifungal mechanism and biological control against citrus pests and diseases. Int. J. Biol. Macromol. 307, 141842. https://doi.org/10.1016/j.ijbiomac.2025.141842.

Yu, K.X., Wong, C.L., Ahmad, R., Jantan, I., 2015. Larvicidal activity, inhibition effect on development, histopathological alteration and morphological aberration induced by seaweed extracts in *Aedes aegypti* (Diptera: culicidae). Asian Pac. J. Tropical Med. 8 (12), 1006–1012. https://doi.org/10.1016/j.apjtm.2015.11.011.

Zhang, W., Ma, J., Yan, Q., Jiang, Z., Yang, S., 2021. Biochemical characterization of a novel acidic chitinase with antifungal activity from *Paenibacillus xylanexedens* Z2–4. Int. J. Biol. Macromol. 182, 1528–1536. https://doi.org/10.1016/j.ijbiomac.2021.05.111.

Zhao, F.F., Wang, S.C., Zhu, Z.L., Wang, S.G., Liu, F.F., Liu, G.Z., 2019. Effects of oxidation degree on photo-transformation and the resulting toxicity of graphene oxide in aqueous environment. Environ. Pollut. 249, 1106–1114. https://doi.org/10.1016/j.envpol.2019.03.114.

Zhou, X., Shi, T., Zhou, H., 2012. Hydrothermal preparation of ZnO-reduced graphene oxide hybrid with high performance in photocatalytic degradation. Appl. Surf. Sci. 258 (17), 6204–6211. https://doi.org/10.1016/j.apsusc.2012.02.131.